

## RESEARCH ARTICLE

10.1002/2013JD021389

## Key Points:

- A global model simulates nitrate deposition from solar proton events
- Soluble ion correlations in Summit snow identify tropospheric sources of nitrate
- Nitrate ions in snow are found not to be a good proxy for solar proton events

## Correspondence to:

K. A. Duderstadt,  
duderstadt@ruston.sr.unh.edu

## Citation:

Duderstadt, K. A., J. E. Dibb, C. H. Jackman, C. E. Randall, S. C. Solomon, M. J. Mills, N. A. Schwadron, and H. E. Spence (2014), Nitrate deposition to surface snow at Summit, Greenland, following the 9 November 2000 solar proton event, *J. Geophys. Res. Atmos.*, *119*, 6938–6957, doi:10.1002/2013JD021389.

Received 18 DEC 2013

Accepted 19 MAY 2014

Accepted article online 24 MAY 2014

Published online 10 JUN 2014

## Nitrate deposition to surface snow at Summit, Greenland, following the 9 November 2000 solar proton event

Katharine A. Duderstadt<sup>1</sup>, Jack E. Dibb<sup>1</sup>, Charles H. Jackman<sup>2</sup>, Cora E. Randall<sup>3</sup>, Stanley C. Solomon<sup>4</sup>, Michael J. Mills<sup>4</sup>, Nathan A. Schwadron<sup>1</sup>, and Harlan E. Spence<sup>1</sup>

<sup>1</sup>Institute for the Study of Earth, Oceans, and Space, University of New Hampshire, Durham, New Hampshire, USA, <sup>2</sup>NASA Goddard Space Flight Center, Greenbelt, Maryland, USA, <sup>3</sup>Laboratory for Atmospheric and Space Physics, University of Colorado Boulder, Boulder, Colorado, USA, <sup>4</sup>National Center for Atmospheric Research, Boulder, Colorado, USA

**Abstract** This study considers whether spikes in nitrate in snow sampled at Summit, Greenland, from August 2000 to August 2002 are related to solar proton events. After identifying tropospheric sources of nitrate on the basis of correlations with sulfate, ammonium, sodium, and calcium, we use the three-dimensional global Whole Atmosphere Community Climate Model (WACCM) to examine unaccounted for nitrate spikes. Model calculations confirm that solar proton events significantly impact HO<sub>x</sub>, NO<sub>x</sub>, and O<sub>3</sub> levels in the mesosphere and stratosphere during the weeks and months following the major 9 November 2000 solar proton event. However, solar proton event (SPE)-enhanced NO<sub>y</sub> calculated within the atmospheric column is too small to account for the observed nitrate peaks in surface snow. Instead, our WACCM results suggest that nitrate spikes not readily accounted for by measurement correlations are likely of anthropogenic origin. These results, consistent with other recent studies, imply that nitrate spikes in ice cores are not suitable proxies for individual SPEs and motivate the need to identify alternative proxies.

### 1. Introduction

Identifying the impact of solar particle storms on the atmosphere remains fundamental in understanding the Sun's influence on Earth's climate [Gray *et al.*, 2010; National Research Council, 2012]. High-energy particles from these solar events increase odd nitrogen and odd hydrogen, catalytically destroying ozone and thereby potentially impacting climate through the chemistry, radiative budget, and dynamics of the upper atmosphere [e.g., Randall *et al.*, 2005; Jackman *et al.*, 2008]. In addition, these space weather events have the potential to disrupt power grids, communications technology, and spacecraft [National Research Council, 2008].

Direct observations of solar energetic particle events have only been available since the midtwentieth century. A broader understanding of the potential frequency and intensity of these events requires a more extensive record of historical occurrences, motivating the search for indirect proxy evidence [Schrijver *et al.*, 2012]. There are numerous analytical and predictive studies using nitrate ion (NO<sub>3</sub><sup>-</sup>) variability in polar ice cores as a proxy for solar energetic particle events [e.g., Zeller and Parker, 1981; Dreschhoff and Zeller, 1990; McCracken *et al.*, 2001a; Shea *et al.*, 2006; Kepko *et al.*, 2009]. However, this relationship has been questioned, particularly with regard to the short timescales associated with individual events [e.g., Legrand and Delmas, 1986; Wolff *et al.*, 2008, 2012]. Contemporary progress toward predicting space weather urgently awaits the resolution of whether or not NO<sub>3</sub><sup>-</sup> spikes in ice cores can be used to infer past events [e.g., Barnard *et al.*, 2011; Riley, 2012].

Zeller and Parker [1981] associated nitrate levels with solar activity through the correlation NO<sub>3</sub><sup>-</sup> in Antarctic ice cores with cosmogenic carbon isotopes (<sup>14</sup>C) in tree rings. Statistical correlation studies confirm the covariance between NO<sub>3</sub><sup>-</sup> and cosmogenic radionuclides <sup>14</sup>C and <sup>10</sup>Be on centennial to millennial timescales [e.g., McCracken *et al.*, 2001b; Traversi *et al.*, 2012; Ogurtsov and Oinonen, 2014]. However, attempts to find a correlation between NO<sub>3</sub><sup>-</sup> and solar variability on smaller timescales, such as the 11 year solar cycle or individual events, have been unsuccessful [e.g., Legrand and Delmas, 1986; Legrand and Kirchner, 1990; Legrand *et al.*, 1996; Traversi *et al.*, 2012]. Instead, the variability of NO<sub>3</sub><sup>-</sup> in polar ice is attributable to lightning from lower latitudes and downward transport from the lower stratosphere [Legrand and Delmas, 1986; Legrand *et al.*, 1989, 1996], with potential contributions in the Arctic from anthropogenic pollution [Mayewski *et al.*, 1990] and biomass burning [e.g., Whitlow *et al.*, 1994; Dibb and Jaffredo, 1997; Savarino and Legrand, 1998].

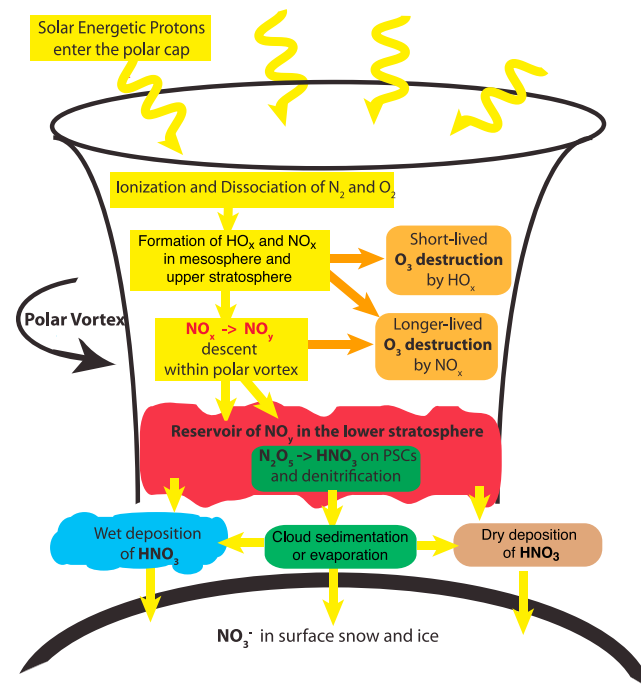


**Figure 1.** Schematic diagram of processes involved with nitrate deposition from solar energetic protons.

Efforts to attribute sharp  $\text{NO}_3^-$  peaks in ice cores to individual solar proton events are exemplified by the *Zeller and Dreschhoff* [1995] analysis of 400 years of nitrate data from the GISP2-H (Greenland Ice Sheet Project 2) Greenland ice core and the estimated cumulative probabilities of solar event occurrences by *McCracken et al.* [2001a]. However, theoretical considerations and model simulations suggest that enhancements of nitrogen species from individual solar events are unlikely to produce sharp peaks in  $\text{NO}_3^-$  at the surface, given the slow rate of vertical transport in the stratosphere, horizontal mixing and dilution to lower latitudes, and diabatic recirculation [e.g., *Legrand et al.*, 1989; *Legrand and Kirchner*, 1990]. In addition, *Weller et al.* [2011] find no indication of individual solar events in 25 years of atmospheric aerosol measurements in Antarctica. Instead, *Wolff et al.* [2008, 2012] are able to attribute  $\text{NO}_3^-$  peaks to tropospheric sources using correlations

among a suite of ions in surface snow. *Palmer et al.* [2001] also do not find a correlation between nitrate spikes and individual solar events in ice cores sampled at Law Dome, Antarctica. However, a statistical analysis reveals an 11% enhancement of  $\text{NO}_3^-$  during the 3 to 14 months following solar events [*Palmer et al.*, 2001].

This paper presents a case study adding to a growing literature that challenges the validity of using nitrate spikes in ice as proxies for individual solar energetic particle events. A three-dimensional global simulation of the 9 November 2000 solar proton event using the Whole Atmosphere Community Climate Model (WACCM) combined with daily samples of  $\text{NO}_3^-$  in surface snow at Summit, Greenland, demonstrates the difficulty in generating impulsive enhancements in nitrate deposition in snow and ice from a single event. The results of this study, however, reiterate the significant influence of solar energetic particles on the chemical composition of the Arctic polar stratosphere and mesosphere, especially levels of odd nitrogen and ozone, encouraging the search for robust proxies other than nitrate to determine the frequency and intensity of historical solar events.

## 2. Methods

### 2.1. Conceptual Description of Solar Proton Events and Nitrate Precursors

Solar energetic particles precipitating into our atmosphere include electrons, protons, and the nuclei of helium and heavier elements. Our study focuses on solar proton events (SPEs), as solar protons uniquely possess sufficient energies to penetrate and modify the chemistry of the mesosphere and stratosphere, potentially leading to chemical signatures within the troposphere and at the surface. Figure 1 presents a schematic of the perturbations caused by solar energetic protons within the polar atmosphere. High-energy protons from solar flares and coronal mass ejections precipitate over the polar caps, commonly extending to geomagnetic latitudes greater than  $60^\circ$  [*Smart and Shea*, 1994]. These high-energy protons, along with collisional secondary electrons, ionize and dissociate molecular nitrogen and oxygen, resulting in the formation of odd hydrogen ( $\text{HO}_x = \text{H} + \text{OH} + \text{HO}_2$ ) and reactive odd nitrogen ( $\text{NO}_x = \text{N} + \text{NO} + \text{NO}_2$ ) [e.g., *Crutzen et al.*, 1975; *Jackman et al.*, 1980; *Solomon et al.*, 1981].

Enhancements of  $\text{HO}_x$  cause short-lived catalytic ozone destruction in the mesosphere and upper stratosphere during an SPE and for a few days following the event [e.g., *Solomon et al.*, 1981; *Jackman et al.*, 2008;

*Damiani et al.*, 2010].  $\text{NO}_x$  has a short lifetime in the upper mesosphere and thermosphere, but the lifetime increases to months during polar night in the stratosphere. During winter, when downward transport within the isolated polar vortex is strong and photochemistry is limited,  $\text{NO}_x$  produced by SPEs in the mesosphere and upper stratosphere can be transported to the middle and lower stratosphere [*López-Puertas et al.*, 2005; *Randall et al.*, 2005; *Jackman et al.*, 2009; *Randall et al.*, 2009]. Loss of  $\text{O}_3$  from the oxidation of SPE-enhanced  $\text{NO}_x$  mainly results in nitric acid ( $\text{HNO}_3$ ) and dinitrogen pentoxide ( $\text{N}_2\text{O}_5$ ). These species eventually mix with the large pool of total odd nitrogen ( $\text{NO}_y = \text{N} + \text{NO}_2 + \text{NO}_3 + 2\text{N}_2\text{O}_5 + \text{HNO}_3 + \text{HO}_2\text{NO}_2 + \text{ClONO}_2 + \text{BrONO}_2$ ) in the lower stratosphere, a background reservoir produced primarily by the oxidation of nitrous oxides ( $\text{N}_2\text{O}$ ) emitted at the surface [*Vitt and Jackman*, 1996]. With the return of sunlight to the polar region,  $\text{NO}_x$  can more effectively destroy stratospheric ozone through catalytic reactions.

Total odd nitrogen species such as  $\text{HNO}_3$ ,  $\text{HO}_2\text{NO}_2$ ,  $\text{ClONO}_2$ , and  $\text{N}_2\text{O}_5$  serve as precursors to  $\text{NO}_3^-$  deposited in snow.  $\text{NO}_3^-$  from  $\text{HNO}_3$ , and to a lesser extent  $\text{HO}_2\text{NO}_2$ , can reach the surface through stratosphere-troposphere exchange followed by wet deposition. In the winter polar vortex, polar stratospheric clouds (PSCs) formed from the cocondensation of nitric acid and water vapor can gravitationally sediment to the troposphere, depending on temperature and particle size. In addition, heterogeneous reactions of  $\text{N}_2\text{O}_5 + \text{H}_2\text{O}$  and  $\text{ClONO}_2 + \text{HCl}$  occur on the surfaces of PSCs to form  $\text{HNO}_3$ , similarly capable of condensing and sedimenting out of the stratosphere. On the basis of inferences from nitrate layers in ice core data, *McCracken et al.* [2001a] and *Shea et al.* [2006] suggest that the deposition of nitrate to the surface resulting from SPEs occurs 2–6 weeks following each event. This contradicts calculations by *Legrand et al.* [1989] that suggest a 2 year transport time of enhanced odd nitrogen from the upper stratosphere to lower stratosphere, a consequence of horizontal diffusion to lower latitudes and vertical diabatic recirculation.

A viable mechanism for SPE nitrate precursors to progress from the upper atmosphere to the surface snow within a 2–6 week timeframe would require the following: (1) rapid downward transport from the upper stratosphere, (2) levels of  $\text{NO}_y$  produced by SPEs high enough to compete with the background reservoir of  $\text{NO}_y$  in the lower stratosphere, and (3) a mechanism for quickly depositing nitrate from the lower stratosphere to the surface. Measurements with high temporal resolution would be necessary to identify these events at the surface. While ice core sampling techniques such as continuous flow analysis [e.g., *Sigg et al.*, 1994; *Röthlisberger et al.*, 2000; *Kepko et al.*, 2009] may achieve this resolution, high-frequency sampling of surface snow (this study) or ambient air [e.g., *Wolff et al.*, 2008; *Weller et al.*, 2011] provides both high resolution as well as limits to postdepositional processing.

Using daily measurements of surface snow at Summit, Greenland, the investigation described in this paper resolves nitrate variability on timescales that should be able to capture an individual SPE. Although there are larger SPE events during meteorological periods of stronger downward transport, we target the SPE of 9 November 2000 because daily surface snow measurements following this event are complete enough to infer alternative tropospheric sources of  $\text{NO}_3^-$  spikes through correlation analysis with sulfate, ammonium, sodium, and calcium (as discussed in section 3.1). The 9 November 2000 event is the sixth largest SPE in the last 50 years with respect to the calculated production of  $\text{NO}_y$ , three times weaker than the largest event on 19–27 October 1989 [*Jackman et al.*, 2008]. This study searches for a one-to-one correspondence between nitrate spikes and solar proton events and does not address longer-term statistical elevations of nitrate and the potential association with solar activity [e.g., *Palmer et al.*, 2001; *Motizuki et al.*, 2009; *Traversi et al.*, 2012; *Ogurtsov and Oinonen*, 2014].

## 2.2. The Whole Atmosphere Community Climate Model

The Whole Atmosphere Community Climate Model (WACCM) is a component of the Community Earth System Model (CESM) at the National Center for Atmospheric Research (NCAR). Model documentation is available at the CESM website ([www2.cesm.ucar.edu](http://www2.cesm.ucar.edu)). Simulations in this study use version cesm1.0.5 (WACCM4), with active atmospheric and land models, prescribed ice, and fixed ocean (specified sea surface temperatures). The WACCM atmospheric component of the model combines the Community Atmosphere Model (CAM5), the thermosphere-ionosphere-mesosphere electrodynamics general circulation model, and the Model for OZone And Related chemical Tracers (MOZART) to simulate dynamics and chemistry from the surface to the lower thermosphere [*Garcia et al.*, 2007; *Kinnison et al.*, 2007; *Emmons et al.*, 2010; *Marsh et al.*, 2013; *Neale et al.*, 2013].

The chemical solver and reaction rates are based on MOZART chemistry [Kinnison *et al.*, 2007; Emmons *et al.*, 2010]. Observed solar spectral irradiance and geomagnetic activity force the heating and photolysis rates [Marsh *et al.*, 2007]. The chemical mechanism includes 59 species and involves reactions of  $O_x$ ,  $NO_x$ ,  $HO_x$ ,  $ClO_x$ , and  $BrO_x$  chemical families as well as methane and carbon monoxide oxidation. The mechanism contains heterogeneous reactions on stratospheric aerosols, including liquid sulfate aerosols along with nitric acid trihydrate (NAT), supercooled ternary solution (STS), and water ice associated with PSCs [Kinnison *et al.*, 2007]. Concentrations of longer-lived greenhouse gases and halogen species are specified from observations [Garcia *et al.*, 2007]. Surface emissions are represented by flux boundary conditions associated with the most recently available compilation supported by WACCM and described by Lamarque *et al.* [2012]: anthropogenic emissions from POET (precursors of ozone and their effects on the troposphere) [Granier *et al.*, 2005] and regional emissions inventory in Asia; monthly biomass burning emissions from Global Fire Emissions Database version 2 [van der Werf *et al.*, 2006]; and biogenic, soil, ocean, and volcanic emissions from POET and the Global Emissions Inventory Activity. These inventories correspond to emissions used in the Coupled Model Intercomparison Project phase 5 (CMIP5) [Taylor *et al.*, 2012].

The WACCM simulations used here have a resolution of  $1.9^\circ$  latitude,  $2.5^\circ$  longitude, and 88 vertical layers extending from the surface to approximately 140 km. The model chemistry applies 30 min time steps. We use the specified dynamics version of WACCM in which meteorology is forced by NASA's Modern Era Retrospective Analysis for Research Applications (MERRA) fields [Rienecker *et al.*, 2011]. WACCM achieves this forcing by relaxing horizontal winds and temperatures to MERRA fields from 0 to 40 km. The model is free running above 50 km, with a linear reduction of forcing between 40 and 50 km.

WACCM modelers have participated in a series of intercomparisons and validation studies, most recently CMIP5 [Taylor *et al.*, 2012]. Funke *et al.* [2011] include WACCM in an intercomparison focused on the SPEs of October 2003, validating results with observations from the Michelson Interferometer for Passive Atmospheric Sounding (MIPAS) on Envisat. There is good agreement between model calculations and measurements, including  $O_3$  loss within 5% and model  $NO_y$  enhancement within 30% at 1 hPa [Funke *et al.*, 2011].

Previous WACCM simulations studying SPEs include Jackman *et al.* [2008, 2009, 2011] and Funke *et al.* [2011]. The WACCM simulations presented in this paper are motivated in part by Figure 6 from Jackman *et al.* [2009], showing a tongue of enhanced  $NO_y$  and decreased  $O_3$  extending into the northern polar lower stratosphere following the 9 November 2000 SPE. The present simulations differ by (1) forcing the model with MERRA reanalysis meteorological fields specific to the 2000–2001 time period, (2) using a more recent version of WACCM with improvements including parameterizations for wave interactions resulting from turbulent mountain stress, and (3) using a higher horizontal resolution to better resolve transport ( $1.9^\circ$  latitude  $\times$   $2.5^\circ$  longitude in contrast to the Jackman *et al.* [2009]  $4^\circ$  latitude  $\times$   $5^\circ$  longitude).

### 2.3. Modeling the 9 November 2000 Solar Proton Event

Following a coronal mass ejection on 8 November 2000 (23:26 UTC), the GOES 8 satellite measured a solar proton event (SPE) beginning on 8 November (23:50 UTC) and reaching a maximum on 9 November (15:55 UTC). A smaller event occurred in late November, peaking on 26 November (20:30 UTC). The proton flux for energies greater than 10 MeV reach a maximum of 14,800 pfu (pfu = proton flux units = particles  $sr^{-1} cm^{-2} s^{-1}$ ) for the 9 November event and 940 pfu for the 26 November event (<http://www.swpc.noaa.gov>).

The WACCM model assumes a uniform distribution of proton flux at geomagnetic latitudes greater than  $60^\circ$ , using calculations of daily averaged ion pair production rates as a function of pressure based on GOES 8 proton flux measurements [Jackman *et al.*, 1980, 2005, 2008]. WACCM includes  $HO_x$  production rates as a function of altitude and ion pairs using a table from Jackman *et al.* [2005] based on the ionization of  $N_2$  and  $O_2$  followed by water cluster ion formation and neutralization described by Solomon *et al.* [1981].  $NO_x$  formation results from the ionization and dissociation of  $N_2$  and  $O_2$ , producing  $\sim 1.25$  N per ion pair [Porter *et al.*, 1976] partitioned into 45% ground state  $N(^4S)$  and 55% excited state  $N(^2D)$ . The excited state  $N(^2D)$  determines net  $NO_x$  production [Rusch *et al.*, 1981]. Tabulated calculations and detailed descriptions of  $NO_x$  and  $HO_x$  production rates by SPEs are available at the Solar Influences for Stratospheric Processes and their Role in Climate website (<http://solarisheppa.geomar.de/solarisheppa/solarprotonfluxes>).

WACCM calculations of gas phase chemical species include loss rates for dry deposition, wet deposition, and heterogeneous reactions on stratospheric aerosols. Dry deposition follows a resistance approach, dependent on land cover type and surface roughness. WACCM calculates the dry deposition flux for a given species as the product of deposition velocities (varying by time and horizontal grid location) and concentrations at a reference height (~10 m) above the surface.

There are two wet deposition schemes available for WACCM: the traditional MOZART scheme [Rasch *et al.*, 1997; Horowitz *et al.*, 2003] and a more extensive scheme detailed by Neu and Prather [2012]. The MOZART scheme addresses convective updrafts, in-cloud nucleation scavenging (rainout), below-cloud impaction scavenging (washout), and evaporation in clear ambient air. Precipitation rates, cloud water content, and cloud fractions are taken from meteorological data fields, and effective Henry's law coefficients are prescribed. The Neu and Prather [2012] wet deposition scheme includes a more resolved subgrid scale treatment of cloud overlap and a burial method for the uptake of soluble gases on ice, resulting in slower uptake of HNO<sub>3</sub> by ice and snow. This study uses the MOZART scheme in an effort to provide an upper limit for wet deposition of HNO<sub>3</sub>, consistent with the search for the maximum potential deposition of nitrate following SPEs.

WACCM treats wet deposition as a first-order gas phase loss process at the end of each time step. The model does not explicitly account for the accumulation of condensed species within cloud droplets or aqueous chemistry, nor does it archive soluble ions deposited to the surface. The results presented in this paper estimate the variability in nitrate deposition by integrating gas phase loss through wet deposition over the total atmospheric column and then dividing by precipitation amounts, filtering model output when precipitation values are extremely low to prevent anomalous spikes. These calculations are expected to overestimate the magnitude of NO<sub>3</sub><sup>-</sup> deposited to the snow but allow a comparison of modeled variability in nitrate deposition with observed variability in surface snow measurements.

WACCM also calculates the uptake of HNO<sub>3</sub> by stratospheric aerosols and the gravitational settling of stratospheric cloud particles (as described in Kinnison *et al.* [2007] and Wegner *et al.* [2013]). Combining the sedimentation of condensed phase HNO<sub>3</sub> with the heterogeneous conversion of N<sub>2</sub>O<sub>5</sub> to HNO<sub>3</sub> on polar stratospheric clouds allows WACCM to calculate the contribution of nitrate to the troposphere through irreversible denitrification of the stratosphere.

#### 2.4. Observations of Nitrate in Surface Snow at Summit, Greenland

Summit Station, originally the site of the Greenland Ice Sheet Project 2 (GISP2), is located in the middle of the Greenland ice sheet, approximately 3200 m above sea level at 72°34'N latitude and 38°29'W longitude. Atmospheric measurements have been made at the site since 1989, with a variety of intensive measurements throughout the 1980s and 1990s, culminating in a full suite of continuous measurements beginning in 2003 as part of the Arctic Observing Network (<http://www.geosummit.org>).

Year-round daily measurements of soluble ion content in surface snow are available during 1997–1998 and from August 2000 to August 2002 [Dibb *et al.*, 2007]. Vertical profiles from monthly 1 m snow pits accompany these measurements. Determined ions include sodium (Na<sup>+</sup>), ammonium (NH<sub>4</sub><sup>+</sup>), potassium (K<sup>+</sup>), magnesium (Mg<sup>2+</sup>), calcium (Ca<sup>2+</sup>), chloride (Cl<sup>-</sup>), nitrate (NO<sub>3</sub><sup>-</sup>), and sulfate (SO<sub>4</sub><sup>2-</sup>). Sampling procedures, transport and storage, and ion chromatography techniques and uncertainties are described in detail by Dibb *et al.* [2007], following protocols summarized by Wolff [1995]. Briefly, snow was sampled daily from an area upwind of Summit camp to avoid contamination from local sources. Samples from the uppermost stratigraphic layer were collected in groups of three adjacent replicates, with companion blanks generated every nine samples. Samples remained at -20°C until analysis, melted in small batches and immediately analyzed by ion chromatography.

The quality of chemical profiles used to infer historical atmospheric conditions such as the influence of solar proton events depends on preservation within the snowpack. The analysis of surface snow and snow pit data reveals that levels of most ions are preserved (at approximately 80%) in layers within the snow pits [Dibb *et al.*, 2007]. The exception is nitrate, where postdepositional processes may significantly modify NO<sub>3</sub><sup>-</sup> concentrations [Dibb *et al.*, 2007]. Evidence of postdepositional modifications has been observed in Greenland as well as in Antarctica [e.g., Dibb and Whitlow, 1996; Dibb and Jaffrezo, 1997; Röthlisberger *et al.*, 2002], with significant differences expected among sites as a result of the physical and chemical environments. These modifications involve snow-air exchange attributed to photolysis, sublimation and condensation associated with the growth of snow grains, and the uptake and release of volatile species such as nitric acid

[e.g., Legrand *et al.*, 1996; Sturm and Benson, 1997; Honrath *et al.*, 1999; Dibb *et al.*, 2002; Grannas *et al.*, 2007]. Traversi *et al.* [2012] suggest that ideal conditions for preserving nitrate in firn with respect to postdepositional effects involve accumulation rates above 50 mm water equivalent per year. While sites in Greenland such as Summit are well above this threshold, many Antarctic plateau sites fall below the limit, including Vostok and Dome C [Traversi *et al.*, 2012, and references therein]. In addition, long periods between snowfalls may allow significant postdepositional processing near the surface.

Postdepositional modifications also depend on the chemical composition of air near the surface, the composition of the snow (particularly with regard to acidity), and the altitude and temperature of the site [e.g., Röthlisberger *et al.*, 2000; Burkhardt *et al.*, 2004]. Recent measurements of oxygen isotopes of nitrate at Summit suggest that postdepositional photolysis of nitrate in surface snow is limited (~2% in summer) [Fibiger *et al.*, 2013]. Furthermore, in the absence of solar radiation, we would not expect postdepositional loss process involving photochemistry and thermal desorption to extensively reduce concentrations during the polar winter. However, modifications of  $\text{NO}_3^-$  levels may result from the migration, diffusion, and chemistry associated with the physical evolution of the snowpack, particularly with regard to the metamorphism and compaction of grains [Bartels-Rausch *et al.*, 2012].

The seasonal cycles of long-lived chemical tracers, greenhouse gases, and nonmethane hydrocarbons demonstrate that Summit is representative of well-mixed, remote Arctic air, with most organic compounds in their final stage of oxidation [Dibb *et al.*, 2007]. Kahl *et al.* [1997] analyze 44 years of 10 day back trajectories at 700 hPa (the elevation of Summit) as well as 500 hPa (5–6 m above mean sea level, reflecting midtropospheric circulation). Westerly flow dominates at Summit during winter, with trajectories originating from North America and the North Pacific (27% at 500 hPa and 91% at 700 hPa) as well as Europe and Asia (70% at 500 hPa and 7% at 700 hPa).

Summit receives ~65 cm of snow (~24 cm water equivalence) per year, with snow accumulation reaching a maximum in spring and a minimum in winter [Dibb and Fahnstock, 2004]. Periods of fresh snow are relatively infrequent during the 2000–2001 winter: six events in November 2000 (0.72 cm water equivalence), two events in December 2000 (0.29 cm water equivalence), and two events in January 2001 (0.56 cm water equivalence). In addition to fresh snow events, field notes indicate frequent periods of thick fog and rime, ice crystals and diamond dust, as well as high winds and blowing snow strong enough to obscure visibility.

### 3. Results and Discussion

#### 3.1. Correlations Between Nitrate and Other Ions in Surface Snow at Summit

Concurrent measurements of nitrate with other ions such as sulfate, calcium, sodium, and ammonium provide a means for attributing nitrate spikes in snow to tropospheric sources, either by direct association with industrial pollution and biomass burning plumes from Europe and North America or from increased nitrate deposition involving particulates such as sea salt and dust. Mayewski *et al.* [1990] credit a rising trend in both  $\text{NO}_3^-$  and  $\text{SO}_4^{2-}$  in Greenland to industrial continental pollution. Anthropogenic pollution not only is characterized by high levels of  $\text{HNO}_3$  but also is the dominant source of sulfate in comparison to sea salt, dust, volcanoes, and biogenic emissions. Chemical signatures of continental biomass burning include elevated levels of  $\text{NH}_4^+$  and formate in Greenland ice, with concurrent enhancements of  $\text{NO}_3^-$  present in some events and absent in others [e.g., Legrand *et al.*, 1992; Whitlow *et al.*, 1994; Legrand and de Angelis, 1996; Savarino and Legrand, 1998]. Dibb *et al.* [1996] and Dibb and Jaffrezo [1997] confirm biomass burning in Northern Canada as a source of enhanced  $\text{NH}_4^+$ , carboxylic acids, and  $\text{NO}_3^-$  at Summit using back trajectories in conjunction with atmospheric and snow measurements.

Observations of atmospheric aerosols at Summit near ground level (1.5 m) show minimal concentrations of particulate nitrate, often below the detection limit of instruments, suggesting that most of nitrate present in snow originates from gas phase  $\text{HNO}_3$  [Silvente, 1993; Silvente and Legrand, 1995; Dibb *et al.*, 1994, 1998]. Contemporaneous measurements at Summit during the summer of 1993 show mean gas phase  $\text{HNO}_3$  concentrations of  $0.9 \pm 0.6 \text{ nmol/m}^3$ , an order of magnitude larger than mean atmospheric aerosol nitrate concentrations of  $0.06 \pm 0.6 \text{ nmol/m}^3$  [Dibb *et al.*, 1994].  $\text{N}_2\text{O}_5$  could potentially be an additional source of  $\text{NO}_3^-$  in snow, particularly in winter, when  $\text{N}_2\text{O}_5$  accumulates in the absence of photochemistry and subsequently reacts heterogeneously with the snow [Huff *et al.*, 2011].

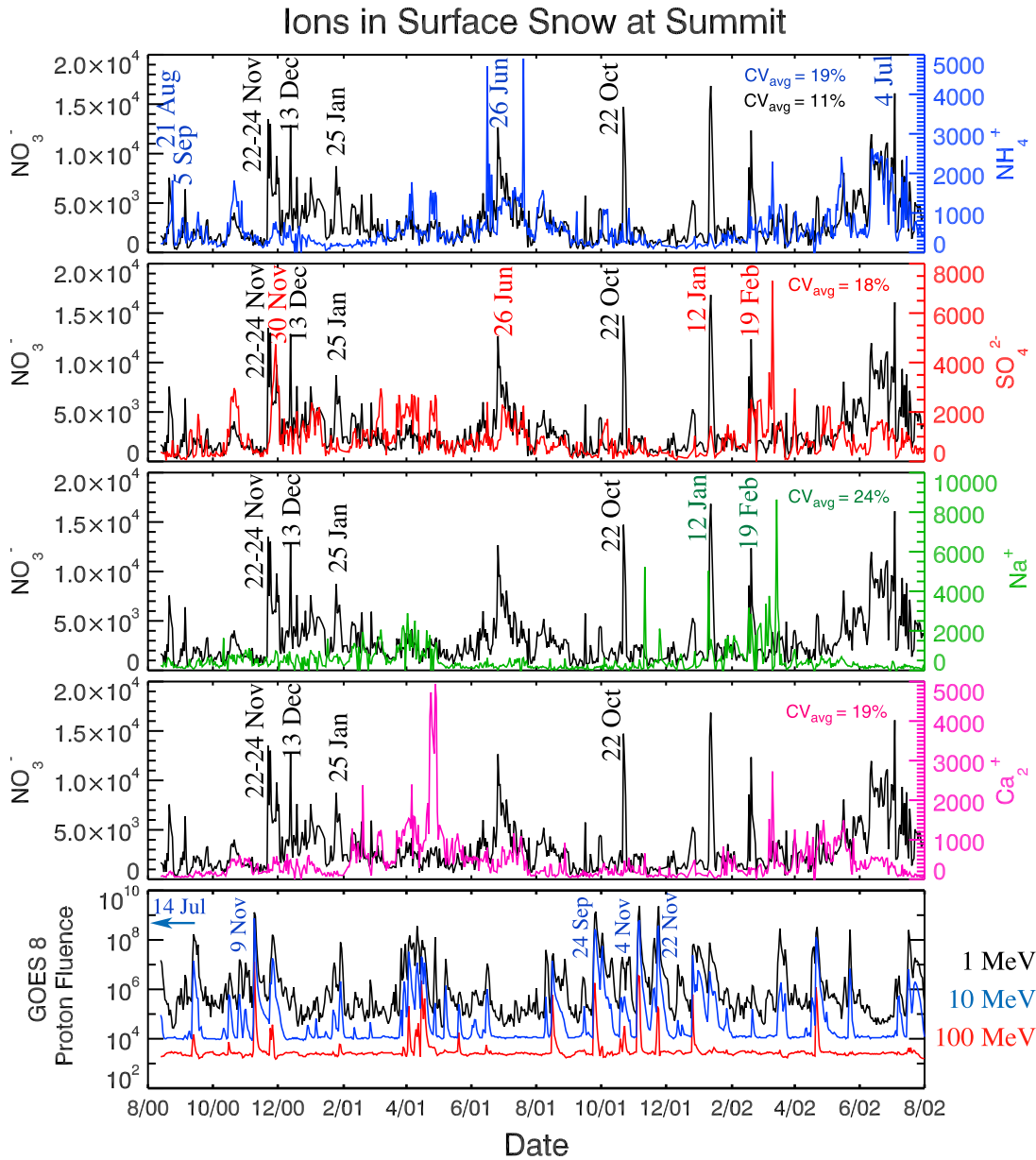


**Figure 2.** Daily measurements of ion content (nmol/kg) in surface snow at Summit, Greenland, from August 2000 to August 2002 [Dibb et al., 2007]. Concurrent peaks of  $\text{NO}_3^-$  and  $\text{NH}_4^+$ ,  $\text{NO}_3^-$  and  $\text{SO}_4^{2-}$ ,  $\text{NO}_3^-$  and  $\text{Na}^+$ , and  $\text{NO}_3^-$  and  $\text{Ca}_2^+$  are dated by color for source identification. Nitrate spikes dated in black represent enhancements not readily attributable to tropospheric sources. The average coefficient of variation ( $\text{CV}_{\text{avg}}$ ) indicates the spread among three simultaneous snow samples used to calculate each daily average, representing the major source of error in the measurements. The lower graph identifies major SPE events in the context of daily solar proton fluxes from GOES 8 in protons  $\text{cm}^{-2} \text{d}^{-1} \text{sr}^{-1}$  (NOAA at <http://www.swpc.noaa.gov/>).

Wolff et al. [2008] attribute correlations between  $\text{NO}_3^-$  and  $\text{Na}^+$  in daily surface snow measurements at Halley, Antarctica, to increased rates of conversion of gaseous to aerosol nitrate on coarse sea-salt aerosols or salty snow surfaces. Wolff et al. [2008] recommend that future analyses of nitrate in snow and ice use ion correlations to screen for known tropospheric sources before searching the residual  $\text{NO}_3^-$  data for potential SPEs. This study adopts such a technique, identifying tropospheric sources through ion correlations at Summit from 2000 to 2002 followed by WACCM model simulations to investigate  $\text{NO}_3^-$  spikes not readily attributable to tropospheric sources.

Figure 2 presents time series plots of  $\text{NO}_3^-$  paired with  $\text{NH}_4^+$ ,  $\text{Na}^+$ ,  $\text{Ca}_2^+$ , and  $\text{SO}_4^{2-}$  at Summit along with solar proton fluxes from GOES 8. Visual examination shows that  $\text{NO}_3^-$  spikes on 21 August 2000, 5 September 2000,

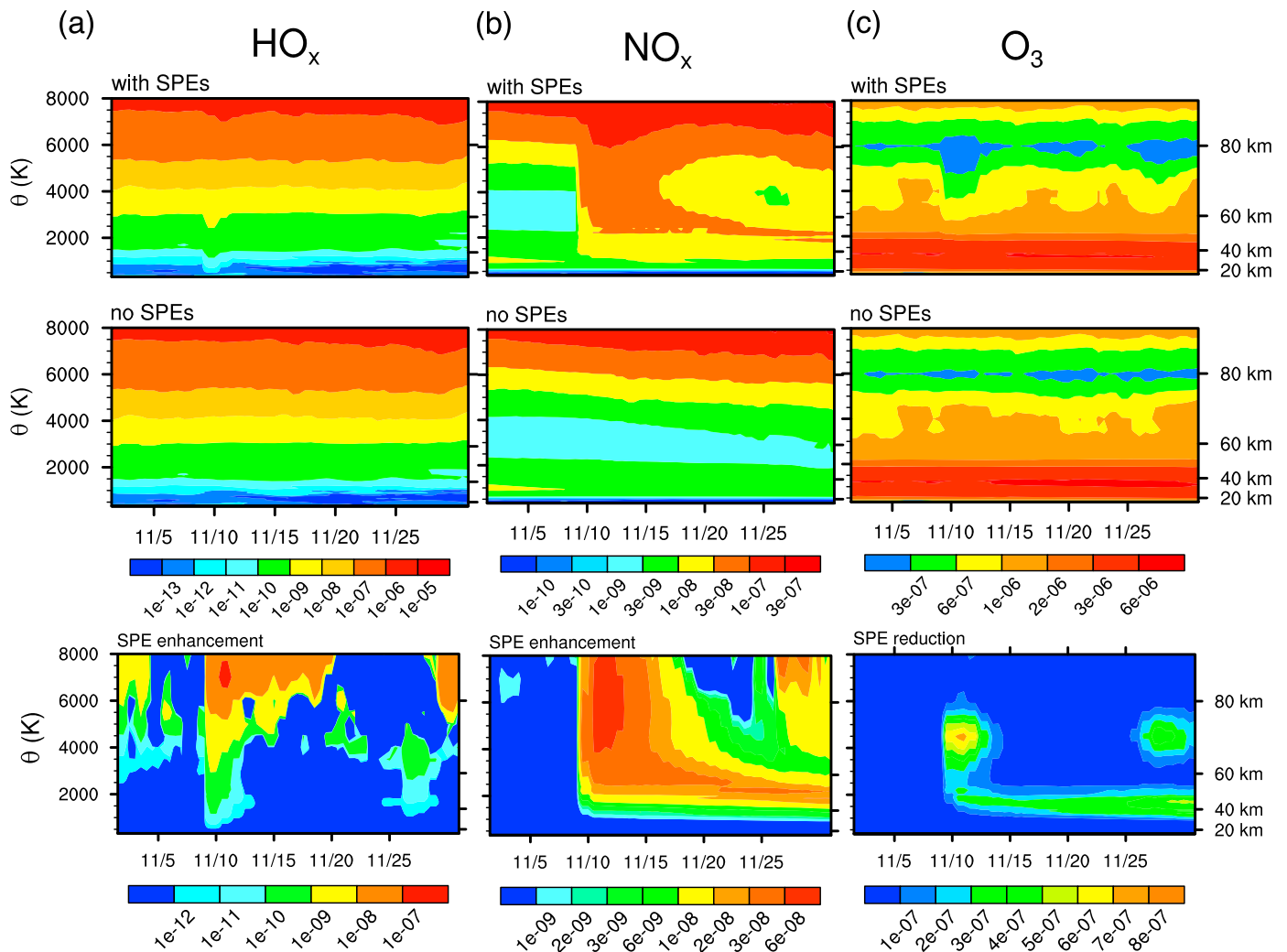


**Figure 3.** Time evolution of the vertical structure for WACCM vortex-averaged (a)  $\text{HO}_x$ , (b)  $\text{NO}_x$ , and (c)  $\text{O}_3$  during the weeks following the 9 November 2000 event (mole ratios). The vertical scale is represented by potential temperature ( $\theta$ ), left, and approximate geopotential height ( $Z$ ), right. Top row: with SPEs. Middle row: no SPEs. Bottom row:  $\text{HO}_x$  enhancement ( $\text{HO}_x$  with SPEs –  $\text{HO}_x$  no SPEs),  $\text{NO}_x$  enhancement ( $\text{NO}_x$  with SPEs –  $\text{NO}_x$  no SPEs), and  $\text{O}_3$  reduction ( $\text{O}_3$  no SPEs –  $\text{O}_3$  with SPEs).

16 June 2001, and 4 July 2002 correlate with  $\text{NH}_4^+$ , a tracer of biomass burning. High levels of the anthropogenic  $\text{SO}_4^{2-}$  accompany nitrate spikes on 25–30 November 2000, 26 June 2001, and 19 February 2002. Levels of  $\text{Na}^+$  associated with sea salt are enhanced along with  $\text{NO}_3^-$  on 12 January 2002 and 19 February 2002. This leaves four  $\text{NO}_3^-$  spikes that are not readily attributable to tropospheric sources: 22–24 November 2000, 13 December 2000, 25 January 2001, and 22 October 2001. The GOES 8 proton fluxes indicate SPEs on 9 November 2000, 24 September 2001, 4 November 2001, and 22 November 2001. This study uses the WACCM model to analyze the three candidate  $\text{NO}_3^-$  spikes that occur during polar winter (22–24 November 2000, 13 December 2000, and 25 January 2001), specifically searching for a potential mechanism to explain how a nitrate signal from the 9 November 2000 SPE might impulsively arrive at the surface through chemistry, transport, and deposition processes within the winter polar vortex.

### 3.2. Modeling the Impact of the 9 November 2000 SPE on $\text{HO}_x$ , $\text{NO}_x$ , and $\text{O}_3$

Comparing WACCM simulations with and without SPEs isolates the impact of solar protons on upper atmospheric processes and identifies potential scenarios leading to enhanced nitrate deposition. The model is initially run from January 2000 through October 2000 to allow chemical species to reach equilibrium throughout the atmosphere, with solar protons (e.g., the 14 July 2000 “Bastille Day” solar proton event) included during this “spin-up” period. At the start of November, the solar proton flux is allowed to continue in a “with SPEs”



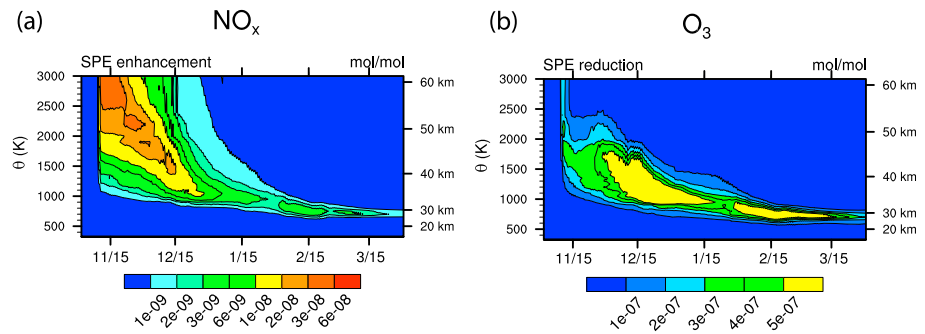


**Figure 4.** Time evolution of the vortex-averaged (a) enhancement of  $\text{NO}_x$  and (b) reduction  $\text{O}_3$  from November through March (mole ratios).

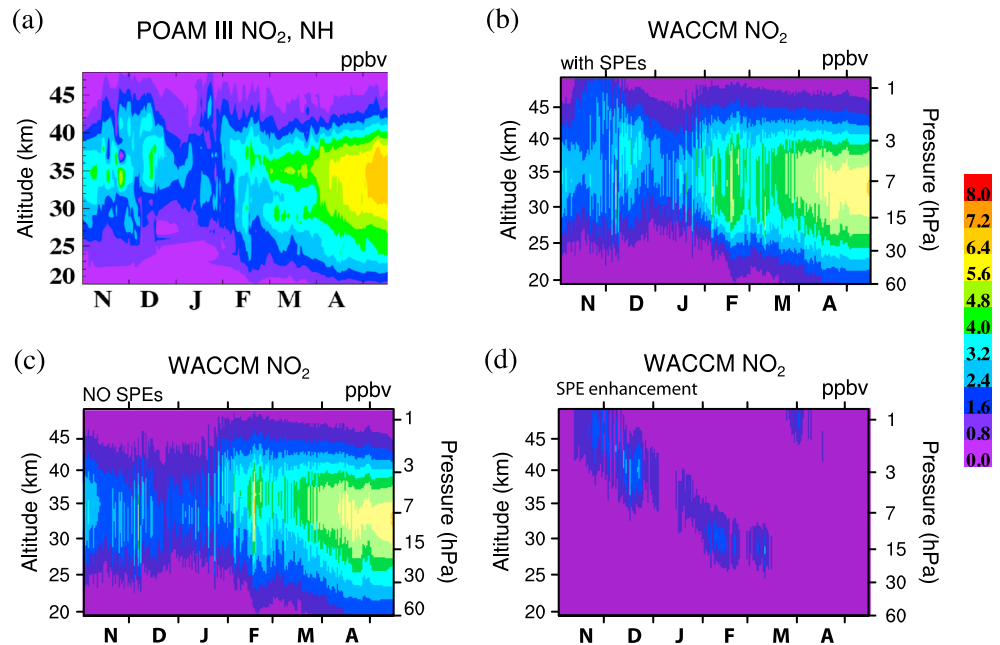
simulation but is set to zero in a “no SPEs” simulation, thereby more effectively highlighting perturbations specific to the 9 November 2000 SPE.

Figure 3 shows the time evolution of the vertical structure of modeled  $\text{HO}_x$ ,  $\text{NO}_x$ , and  $\text{O}_3$  (in mole ratios) during November. Top row shows WACCM simulations with SPEs. Middle row shows WACCM simulations without SPEs. Bottom row shows the SPE enhancements of  $\text{HO}_x$  and  $\text{NO}_x$  and the resulting reduction of  $\text{O}_3$ . These contour plots represent average profiles calculated within the meandering polar vortex, the region most likely associated with strong polar winter descent. Potential temperature ( $\theta$ ) serves as the vertical coordinate on the left axis, while the right axis indicates the approximate geopotential height ( $Z$ ). The boundary of the polar vortex is objectively determined by identifying grid points within the stratosphere where scaled potential vorticity ( $s\text{PV}$ ) calculated on isentropic surfaces exceeds  $1.4 \times 10^{-4} \text{ s}^{-1}$  [Dunkerton and Delisi, 1986; Brakebusch et al., 2013]. Scaled potential vorticity retains the conservation properties of Ertel’s potential vorticity on isentropic surfaces. However, by normalizing with respect to the U.S. Standard Atmosphere [Committee for the Extension of the U.S. Standard Atmosphere, 1976],  $s\text{PV}$  removes vertical disparities in potential vorticity caused by the exponential increase of potential temperature with decreasing pressure. Above 2500 K ( $\sim 55$  km), the vortex is assumed to extend to the same latitudes calculated for 2500 K, as the  $s\text{PV}$  method no longer adequately delineates the vortex edge as a result of the temperature profile above the stratopause.

Figure 3 highlights the significant impact of the 9 November 2000 SPE event on the chemistry of the Arctic mesosphere and stratosphere. Short-lived enhancements up to 100 ppbv  $\text{HO}_x$  occur above 80 km in the mesosphere, with enhancements of 0.1 to 1 ppbv extending throughout the stratosphere during the days following the 9 November SPE (Figure 3a). SPE production of  $\text{NO}_x$  peaks around 50 ppbv in the mesosphere, exceeding 30 ppbv throughout the upper stratosphere during the days following the event (Figure 3b). The  $\text{NO}_x$  enhancements propagate downward within the stratosphere throughout the month, maintaining levels an order of magnitude above background. Losses of  $\text{O}_3$  up to 800 ppbv occur above 70 km immediately following the 9 November SPE (Figure 3c). A 30 to 40% depletion of  $\text{O}_3$  ( $>100$  ppbv) occurs throughout the stratosphere, most likely associated with the short-lived enhancement of  $\text{HO}_x$ .  $\text{O}_3$  reduction continues in the stratosphere throughout the rest of November, consistent with the descent of SPE-enhanced  $\text{NO}_x$ . The smaller SPE at the end of November is also evident in the plots for all three species.

Figure 4 presents the vortex-averaged SPE enhancement of  $\text{NO}_x$  and reduction of  $\text{O}_3$  from November through March.  $\text{NO}_x$  enhancements of 10 to 40 ppbv (10 to 20 times background levels) propagate from the upper stratosphere to the middle stratosphere throughout November and December at a rate of  $\sim 10$  km/month. By January, increases of 3 to 5 ppbv (2 to 3 times background levels) persist from 30 to 35 km, with remnant enhancements continuing into spring.

Figure 4 supports the supposition that the enhancement of  $\text{NO}_x$  during the months following the 9 November SPE drives longer-lived destruction of  $\text{O}_3$  in the stratosphere. The reduction of  $\text{O}_3$  in the stratosphere follows the descent of SPE-enhanced  $\text{NO}_x$ , reaching losses of 500 ppbv during December and early January. Reductions of ozone remain at 400 to 500 ppbv (5 to 10%) from 25 to 30 km until spring. Although most of the ozone reduction occurs above the stratospheric ozone layer, where number densities peak from 15 to 20 km, ozone losses could nonetheless reduce oxidation rates in the middle to lower stratosphere and impact the chemistry, dynamics, and radiative properties of this region.



**Figure 5.** Comparison of WACCM NO<sub>2</sub> with POAM III NO<sub>2</sub> satellite observations: (a) POAM III observations, (b) WACCM with SPEs, (c) WACCM without SPEs, (d) WACCM SPE enhancements (units in ppbv). WACCM results are linearly interpolated and smoothed for clarity during periods when satellite measurements are outside the WACCM polar vortex defined according to  $sPV > 1 \times 10^{-4} s^{-1}$ .

Not surprisingly, the behavior of HO<sub>x</sub>, NO<sub>x</sub>, and O<sub>3</sub> following the 9 November 2000 SPE in these simulations is similar to the *Jackman et al.* [2009] WACCM results. *Jackman et al.* [2009] show an increase in upper stratospheric NO<sub>y</sub> (mostly NO<sub>x</sub>), exceeding 1000% for several days after the 9 November SPE, followed by the prolonged downward transport of enhanced NO<sub>y</sub> during the weeks and months following the event, exceeding 20% at 30 km during January and February. Model calculations of HO<sub>x</sub> and O<sub>3</sub> presented in this paper are also consistent with *Jackman et al.* [2008, 2009].

Figure 5 shows a comparison of NO<sub>2</sub> from WACCM with POAM III (Polar Ozone and Aerosol Measurement) satellite measurements within the Arctic vortex. Descriptions of the POAM III data along with methods for determining the edge of the polar vortex for Figure 5a are provided in *Harvey et al.* [2002] and *Randall et al.* [2002, 2007]. Scaled potential vorticity (sPV) is used to identify the location of the vortex for the WACCM results, consistent with the analysis throughout this paper. Magnitudes of NO<sub>2</sub> simulated by WACCM are similar to observations by POAM III, with background levels 1 to 3 ppbv between 30 and 40 km during November, increasing substantially in early February. The WACCM simulations do a better job capturing levels of NO<sub>2</sub> during December and January when including SPEs. Favorable comparisons for NO<sub>x</sub> and O<sub>3</sub> have also been made among WACCM simulations and available satellite measurements for more recent SPEs, including MIPAS observations of the October 2003 “Halloween” SPEs [*Jackman et al.*, 2008, 2009; *Funke et al.*, 2011] and MIPAS, Microwave Limb Sounder, and Atmospheric Chemistry Experiment-Fourier transform spectrometer observations for the January 2005 SPE [*Jackman et al.*, 2011].

Simulations using global models other than WACCM to study SPEs similar in magnitude to this study also show enhancements of NO<sub>x</sub> and reductions of O<sub>3</sub> in the stratosphere during the months following each event [e.g., *Semeniuk et al.*, 2005; *Päivärinta et al.*, 2013]. *Calisto et al.* [2012] use the SOCOL (European Centre/Hamburg 4 + Solar Climate Ozone Links (SOCOL)) model to study how a hypothetical extremely large SPE (the August 1972 SPE scaled to fluences associated with the 1859 Carrington Event) would impact the atmosphere if it occurred during a contemporary solar maximum. The short-term enhancements of HO<sub>x</sub> (10 ppbv) and NO<sub>x</sub> (200 ppbv) exceed the 9 November 2000 SPE WACCM simulations. However, longer-term increases in NO<sub>x</sub> (10%) and decreases in O<sub>3</sub> (20–40%) in the stratosphere are comparable, likely attributable to solar radiation variations between fall and winter. While the SOCOL simulation of the extreme SPE results in significant depletion of total column O<sub>3</sub> (20 Dobson unit (DU)), the

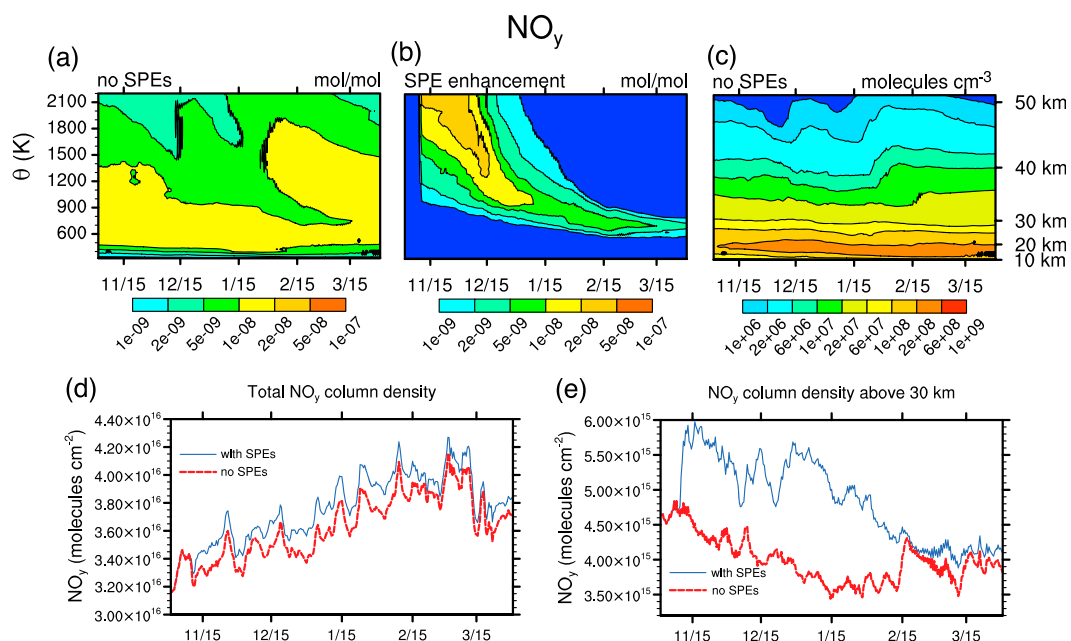
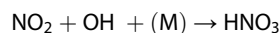


**Figure 6.** WACCM vortex-averaged NO<sub>y</sub>: (a) no SPEs (mole ratios), (b) SPE enhancements (mole ratios), (c) no SPEs (number density), (d) column densities (molecules cm<sup>-2</sup>) integrated throughout the total atmosphere with SPEs (blue) and no SPEs (red), and (e) column densities (molecules cm<sup>-2</sup>) integrate from 30 km to the top of the atmosphere with SPEs (blue) and no SPEs (red).

WACCM simulations of the 9 November SPE show a vortex-averaged decrease reaching only 5 DU by late January, with reductions up to 10 DU occurring sporadically in the center of the vortex.

### 3.3. Modeled Conversion of NO<sub>x</sub> to NO<sub>y</sub> and the Downward Transport of NO<sub>y</sub>

As NO<sub>x</sub> propagates downward within the stratosphere, oxidation reactions convert NO<sub>x</sub> into other NO<sub>y</sub> species, primarily through the following pathways:



(where NO<sub>3</sub> is produced from NO<sub>2</sub> reactions with O and O<sub>3</sub>)

These products of NO<sub>x</sub> oxidation are of particular interest because of their role in nitrate deposition. Background NO<sub>y</sub> densities peak in the lower stratosphere, where a reservoir of HNO<sub>3</sub> accumulates from the oxidation of nitrous oxide (N<sub>2</sub>O) emitted at the surface. The WACCM simulations presented in this paper strive to answer whether or not the NO<sub>y</sub> enhancements resulting from the oxidation of SPE NO<sub>x</sub> can persist with respect to this background pool of NO<sub>y</sub> in the lower stratosphere at levels high enough to be detected at the surface. Note that WACCM does not include reactions involving hydrated cluster ions, which have also been implicated in the production of HNO<sub>3</sub> at altitudes over 35 km [Kawa et al., 1995; Verronen et al., 2008; Kvissel et al., 2012].

Figure 6 presents vortex-averaged NO<sub>y</sub> within the stratosphere from November through March. Figure 6a shows NO<sub>y</sub> in simulations without SPEs, depicting the subsidence of air within the polar vortex during winter. Figure 6b shows the corresponding downward transport of SPE NO<sub>y</sub> enhancements within the stratosphere. By late January there is a thin layer (~5 km) of 5 to 10 ppbv SPE-enhanced NO<sub>y</sub> around 30 km. SPE enhancements continue through March, remaining at altitudes well above 20 km. Figure 6a clearly identifies a background pool of NO<sub>y</sub> in the lower stratosphere (10 to 15 ppbv), an order of magnitude larger than typical values in the middle stratosphere (1 to 4 ppbv) and troposphere (less than 1 ppbv). While downward transport is best studied using mole ratios or mixing ratios (measures of composition that are independent of density), it is nonetheless important to draw attention to the exponential decrease in atmospheric density with height. A background level of 15 ppbv NO<sub>y</sub> at 50 hPa (~20 km) contains a factor of 10 more molecules than 15 ppbv of SPE-enhanced NO<sub>y</sub> at 5 hPa (~35 km). Figure 6c emphasizes that NO<sub>y</sub> background number densities peak below 20 km. The challenge

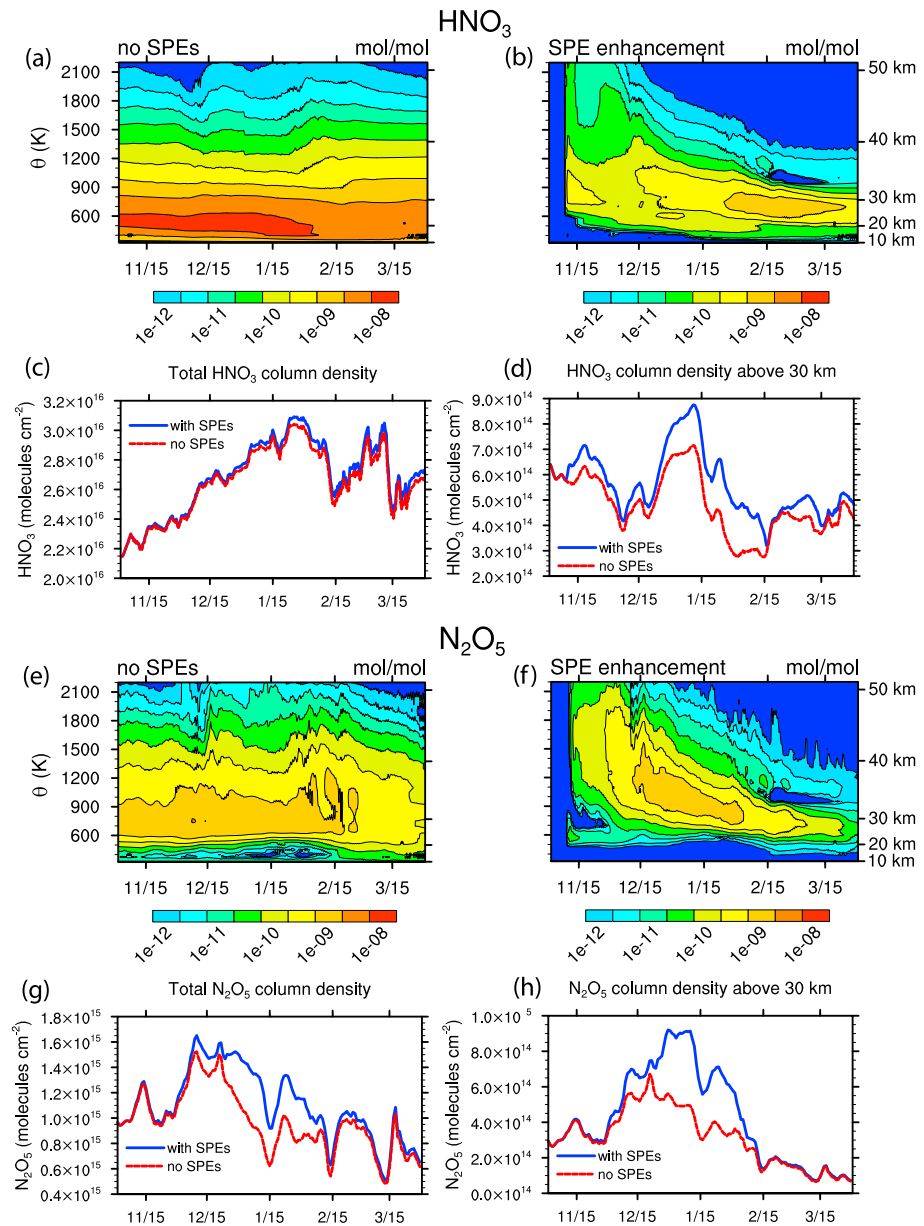


**Figure 7.** Time evolution of WACCM vortex-averaged (a) background  $\text{HNO}_3$  (no SPEs), (b) SPE enhancement of  $\text{HNO}_3$  ( $\text{HNO}_3$  with SPEs –  $\text{HNO}_3$  no SPEs), (c) total column density of  $\text{HNO}_3$ , (d) column density of  $\text{HNO}_3$  above 30 km, (e) background  $\text{N}_2\text{O}_5$  (no SPEs), (f) SPE enhancement of  $\text{N}_2\text{O}_5$  ( $\text{N}_2\text{O}_5$  with SPEs –  $\text{N}_2\text{O}_5$  without SPEs), (g) total column density of  $\text{N}_2\text{O}_5$ , and (h) column density of  $\text{N}_2\text{O}_5$  above 30 km.

remains explaining how a thin SPE-produced layer averaging 5 to 10 ppbv  $\text{NO}_y$  at 30 km might be detected at the surface given the thick background pool of 10 to 15 ppbv  $\text{NO}_y$  in the thermally stable lower stratosphere.

As a means of estimating the maximum potential for enhanced deposition of nitrate at the surface as a result of the 9 November SPE, Figure 6d shows vortex-averaged  $\text{NO}_y$  total column densities from model simulations with SPEs (blue) and without SPEs (red). Vertical column densities are integrated over each model surface grid, and vortex averages are calculated using latitudes and longitudes where sPV values on the 500 K isentropic surface ( $\sim 20$  km) are greater than  $1.4 \times 10^{-4} \text{ s}^{-1}$ . Figure 6e provides similar model results for column densities integrated above 30 km. A large relative increase in column densities above 30 km reflects significant SPE enhancement of  $\text{NO}_y$ . However, the absolute magnitude of the stratospheric SPE-induced  $\text{NO}_y$  enhancement is small compared to the total column density of  $\text{NO}_y$ . There is a general increase in total

column density of  $\text{NO}_y$  throughout winter. However, vortex-averaged SPE enhancements of total column  $\text{NO}_y$  remain below 5%, with enhancements never exceeding 20% at any location within the vortex (not shown). In contrast,  $\text{NO}_3^-$  peaks in snow and ice show enhancements 4 to 5 times background levels, significantly greater than the maximum potential for SPE enhancement suggested by column densities of  $\text{NO}_y$ . The fact that the increase in  $\text{NO}_y$  in the atmospheric column is on average less than 5% (and a maximum of 20% locally) challenges the theory of SPEs being responsible for spikes in  $\text{NO}_3^-$  deposited at the surface.

### 3.4. Modeled Partitioning of $\text{NO}_y$

An analysis of individual  $\text{NO}_y$  species within WACCM helps to identify precursors to  $\text{NO}_3^-$  deposited to the surface. Most of  $\text{NO}_y$  above 40 km is in the form of  $\text{NO}_x$ , while  $\text{HNO}_3$  is the major  $\text{NO}_y$  species below 30 km. Dinitrogen pentoxide ( $\text{N}_2\text{O}_5$ ) becomes significant in the 30 to 40 km layer. Although modeled  $\text{HO}_2\text{NO}_2$  mixing ratios peak in the stratosphere, their contribution to total  $\text{NO}_y$  is less than a few percent.  $\text{HO}_2\text{NO}_2$  contributes most significantly to  $\text{NO}_y$  (~10–15%) in the middle to upper troposphere, where tropospheric  $\text{NO}_x$  and  $\text{HO}_x$  provide a sufficient source of  $\text{HO}_2\text{NO}_2$  and temperatures are low enough to slow thermal decomposition. Other  $\text{NO}_y$  species such as chlorine nitrate ( $\text{ClONO}_2$ ), bromine nitrate ( $\text{BrONO}_2$ ), and nitrate radical ( $\text{NO}_3$ ) are small in comparison.

Figures 7a–7d presents vortex-averaged WACCM simulation results of  $\text{HNO}_3$  including background levels from WACCM simulations without SPEs, enhancements from SPEs, SPE enhancements of column densities integrated over the total atmospheric column, and SPE enhancements of column densities above 30 km. Throughout late December and most of January, SPE enhancements of  $\text{HNO}_3$  do not exceed 1 ppbv, levels much lower than the 10 ppbv background pool of  $\text{HNO}_3$  at 20 km. The largest SPE enhancements of  $\text{HNO}_3$  occur from 20 to 30 km during late January through early March, peaking under 3 ppbv and remaining small in comparison to background values. Vortex-averaged total column densities of  $\text{HNO}_3$  show little change as a result of SPEs, and local enhancements only occasionally reach 2 to 3% within the polar vortex (not shown). The most significant SPE enhancements of  $\text{HNO}_3$  occur above 30 km but have little impact on total column density.

The model calculates an increase in  $\text{N}_2\text{O}_5$  throughout the stratosphere as a result of SPEs (Figures 7e–7h), with most of the enhancement occurring from 30 to 40 km. In contrast to  $\text{HNO}_3$ , the model shows significant enhancements (up to 40%) of vortex-averaged  $\text{N}_2\text{O}_5$  total column density during the months after the 9 November event. Local  $\text{N}_2\text{O}_5$  total column densities are enhanced by over 100% in the center of the vortex during late December and January (not shown).  $\text{N}_2\text{O}_5$  makes up only 5% of total column  $\text{NO}_y$ . In order for total column  $\text{N}_2\text{O}_5$  enhancements to explain  $\text{NO}_3^-$  spikes at the surface, there would need to be a mechanism involving preferential deposition of  $\text{N}_2\text{O}_5$  over  $\text{HNO}_3$ . To the authors' knowledge, no such mechanism has been suggested in the literature. In addition, *Jackman et al.* [2008] and *Funke et al.* [2011] emphasize that WACCM SPE-enhanced  $\text{N}_2\text{O}_5$  is larger than levels from satellite measurements, hypothesizing the need to include water cluster ion reactions in WACCM to convert  $\text{NO}_3$  to  $\text{HNO}_3$  in order to simulate lower  $\text{N}_2\text{O}_5$  values [e.g., *Solomon et al.*, 1981; *López-Puertas et al.*, 2005]. This additional  $\text{HNO}_3$ , however, would not significantly impact the variability of nitrate at the surface, since  $\text{N}_2\text{O}_5$  comprises such a small percentage of total column  $\text{NO}_y$ .

### 3.5. Modeled Deposition of $\text{NO}_y$

Several mechanisms allow nitrogen in the atmosphere to deposit as  $\text{NO}_3^-$  to surface snow. Dry deposition involves gas phase and particulate nitrogen species sticking to the surface snow in the absence of precipitation. Wet deposition removes  $\text{NO}_3^-$ , as  $\text{HNO}_3$  (and to a lesser extent  $\text{HO}_2\text{NO}_2$ ) is taken up by falling snow by means of in-cloud nucleation scavenging and below-cloud impaction scavenging. Nitrate deposition can also result from the uptake of  $\text{HNO}_3$  by polar stratospheric clouds (PSCs), heterogeneous conversion of  $\text{N}_2\text{O}_5$  to  $\text{HNO}_3$  on PSCs, and subsequent gravitational settling of cloud particles to the troposphere.

Although background levels of  $\text{NO}_y$  are large in the lower stratosphere, thermal stability inhibits mixing across the tropopause. In the absence of stratospheric intrusions, denitrification by gravitational settling of PSC particles is the most likely mechanism for upper atmospheric  $\text{NO}_3^-$  to reach the troposphere. WACCM relies on an equilibrium approach to calculate the amount of  $\text{HNO}_3$  condensed on polar stratospheric clouds, which in turn determines the radii and settling velocities of these aerosols (see supporting information in *Kinnison et al.* [2007]). Although heterogeneous reactions in WACCM occur on PSCs composed of supercooled ternary solutions (STS), nitric acid trihydrate (NAT), and water ice [*Kinnison et al.*, 2007; *Lamarque et al.*, 2012; *Wegner et al.*, 2013], condensed nitrogen is limited to STS and NAT aerosols in

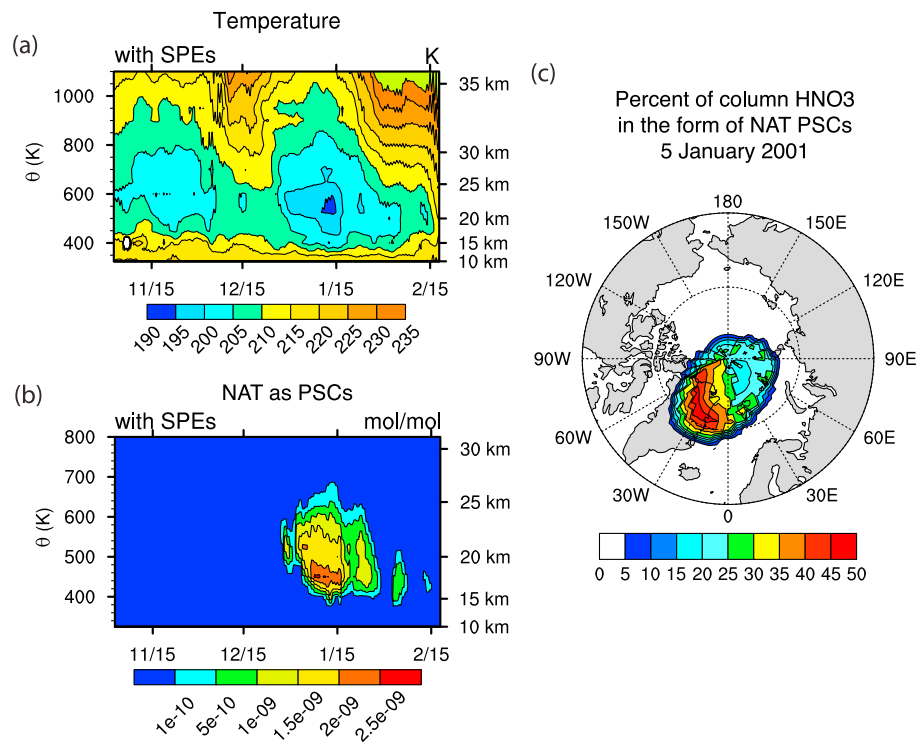


**Figure 8.** WACCM vortex-averaged vertical profiles for (a) temperature (K) and (b) condensed nitrate as nitric acid trihydrate (NAT) PSC particles (mole ratios). (c) Vortex-averaged percent of total column NAT in the form of PSCs with respect to total gas plus condensed phase  $\text{HNO}_3$ . Although results are from simulations with SPEs, differences with respect to simulations without SPEs are negligible.

WACCM, with gravitational settling occurring only for NAT particles because of their larger radii. Once settling and advection bring condensed  $\text{HNO}_3$  to the troposphere, it may be removed from the modeled atmosphere via wet deposition.

Denitrification through cloud sedimentation is not as common in the Arctic as in the Antarctic, where temperatures are low enough to allow PSC particles to grow to larger masses. Although PSCs and denitrification have been observed in the Arctic during years when the polar vortex is strong [e.g., Waibel *et al.*, 1999; Kondo *et al.*, 2000; Santee *et al.*, 2000; Fahey *et al.*, 2001; Popp *et al.*, 2001], the winter of 2000–2001 exhibits neither a consistently strong vortex nor low temperatures (see Figure 1 from Manney *et al.* [2006]). In addition, observations show significant renitrification in the Arctic as increasing temperatures in the lower stratosphere and troposphere cause nitric acid from PSCs to reenter the gas phase [Dibb *et al.*, 2006].

Nonetheless, for completeness, it is useful to consider model-calculated PSCs when examining maximum potential nitrate deposition from the stratosphere. WACCM calculates the presence of all three types of PSCs over the Arctic during winter 2000–2001, with STS and NAT particles most abundant in mid-January and ice clouds briefly present when stratospheric temperatures reach a minimum. Figure 8 presents vortex-averaged vertical temperatures, vortex-averaged condensed nitrate as NAT particles (the most relevant PSC leading to denitrification in WACCM), and condensed nitrate as NAT PSCs for 5 January 2001 (a representative day when PSCs are significant). Although results are given for simulations with SPEs, differences in temperature from simulations without SPEs are negligible and can be attributed to computational noise. WACCM temperatures drop below 200 K during January, reaching a minimum of 194 K at 20 km.

Condensed NAT in the form of PSCs peaks above 15 km during January, contributing 50% of total column  $\text{HNO}_3$  on 5 January 2001. However, NAT radii are small (median radii less than 1.5  $\mu\text{m}$ ), and the modeled flux of nitrate does not extend below 17 km, as temperatures exceed 200 K and condensed nitrate ions reenter the gas phase before reaching the troposphere. The impact of solar proton events on simulated vortex-averaged total column condensed NAT as PSCs is less than 0.2%, with local maximum enhancements of 1 to

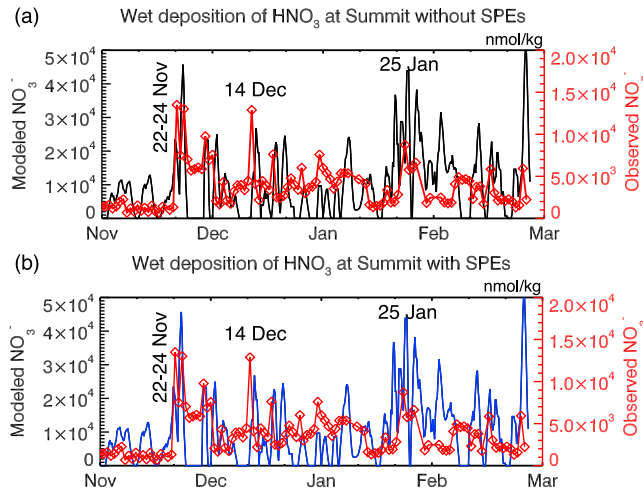


**Figure 9.** Estimates of nitrate from wet deposition at Summit, Greenland, during the 2000–2001 winter (nmol/kg). The blue and black lines along with the left axes show  $\text{NO}_3^-$  resulting from the loss of  $\text{HNO}_3$  in precipitation throughout the atmospheric column during WACCM simulations (a) with SPEs and (b) without SPEs. The red lines and right axes refer to measurements of  $\text{NO}_3^-$  in daily samples of surface snow.

3%. The limited impact of SPEs on nitrate in the form of NAT PSCs is consistent with the limited SPE enhancement of total  $\text{HNO}_3$  presented in Figure 7. In summary, it is unlikely that SPE-enhanced denitrification could account for the fourfold to fivefold  $\text{NO}_3^-$  spikes observed in Greenland surface snow.

Enhanced nitrate from the lower stratosphere enters the troposphere not only through the gravitational settling of PSCs but also from dynamics associated with stratosphere-troposphere exchange. Given the minimal SPE enhancement of  $\text{NO}_y$  in the lower stratosphere, downward transport of SPE-enhanced  $\text{NO}_y$  through isolated tropopause folds and stratospheric intrusions could still not explain the magnitude of observed  $\text{NO}_3^-$  spikes.

In spite of WACCM’s inability to calculate enhancements of  $\text{NO}_y$  from the 9 November 2000 SPE large enough to explain surface spikes in  $\text{NO}_3^-$ , it is nonetheless worthwhile to examine how closely WACCM’s calculations of nitrate deposition resemble observations. Summertime estimates of the  $\text{NO}_3^-$  inventory presented by *Bergin et al.* [1995] attribute 93% of deposition to snow, 6% to fog, and 1% to dry deposition. The strong stability of the wintertime surface layer would suggest that dry deposition plays an even less significant role during the time period

considered in this study. Consequently, our analysis of nitrate deposition will focus solely on wet deposition.

WACCM treats wet deposition in the troposphere as a first-order loss rate from the gas phase, with precipitation rates and cloud cover derived from MERRA meteorological fields. During each time step, WACCM calculates how much of a given gas will be incorporated into cloud droplets and ice crystals within each grid box and removes this amount from the grid box concentration that is passed to the next time step. While reevaporation and desorption are included within a given time step, WACCM does not archive and propagate the soluble ion species nor account for subsequent aqueous reactions. The following analysis assumes that all loss from the gas phase in the tropospheric grid column ends up in precipitated water at the end of each half-hour time step. This analysis estimates the potential enhancement of  $\text{NO}_3^-$  at the surface

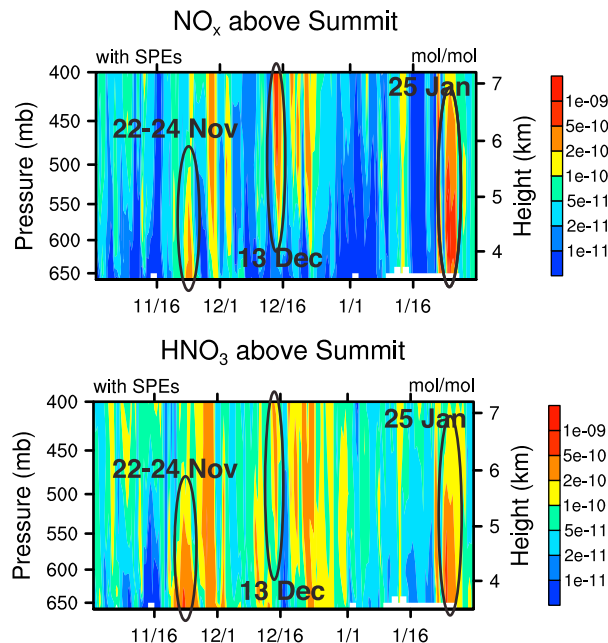


**Figure 10.** WACCM time evolution of the vertical profiles of (top)  $\text{NO}_x$  and (bottom)  $\text{HNO}_3$  above Summit, Greenland. Recall that Summit is located 3.2 km above sea level with surface pressures from 660 to 680 hPa. Peak  $\text{NO}_x$  and  $\text{HNO}_3$  are circled during time periods where surface snow measurements indicate that nitrate ion spikes are not correlated with other ions.

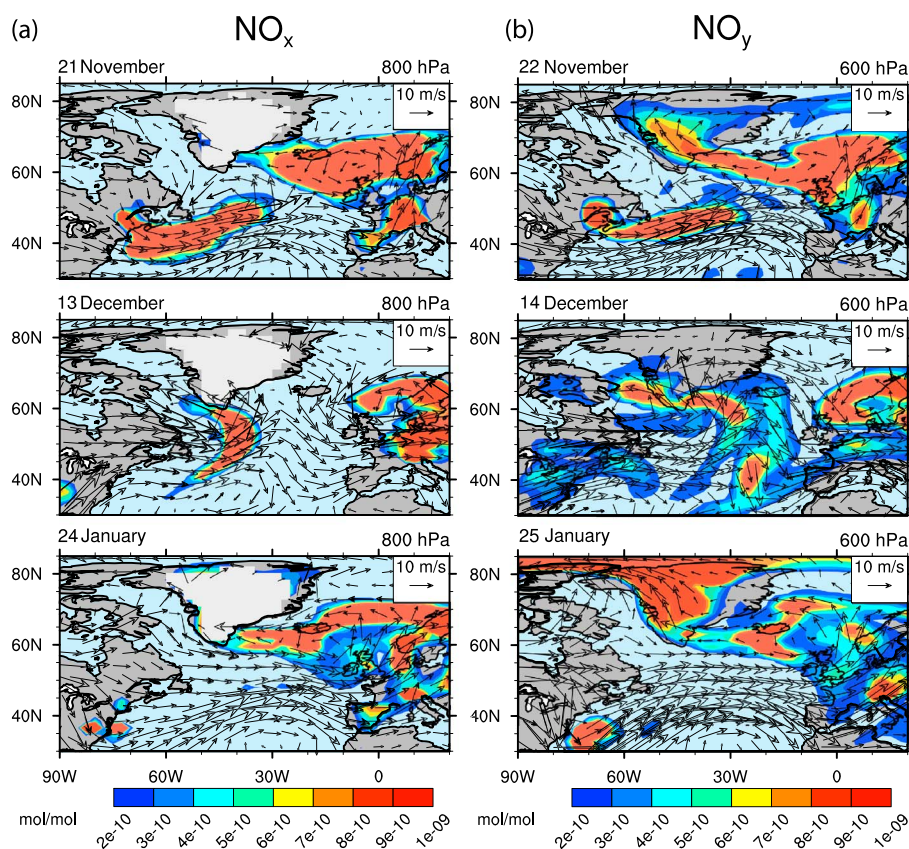


**Figure 11.** The transport of polluted continental plumes simulated by WACCM prior to nitrate ion spikes in Summit snow on 22–24 November, 14 December, and 25 January. (a)  $\text{NO}_x$  at 800 hPa ( $\sim 1.5$  km) on 21 November, 13 December, and 24 January. The white region over Greenland indicates surface elevations above 800 hPa. (b)  $\text{NO}_y$  at 600 hPa ( $\sim 3.5$  km) on 22 November, 14 December, and 25 January. Wind vectors are overlaid on both plots to indicate the travel direction of the polluted plumes.

by wet deposition within the entire vertical tropospheric column, most likely an overestimate especially when precipitation levels are minimal.

Figure 9 shows estimates for nitrate deposition resulting from the wet deposition of  $\text{HNO}_3$  in WACCM directly over Summit both with and without SPEs. The method of calculating modeled wet deposition instantaneously from the entire atmospheric column is useful for determining the maximum potential deposition of nitrate but will tend to overestimate nitrate deposition, as is apparent from the different scales on the left and right vertical axes. This variation in magnitude is confounded by a model grid that is unable to represent the spatial variability caused by blowing or drifting snow, local accumulation and ablation, or sporadic fog and rime at the surface. Instead, our interest lies in identifying whether or not the model can capture the relative variability associated with the measured  $\text{NO}_3^-$ . Indeed, the model does capture relative peaks in nitrate on 23 November, 14 December, and 24 January corresponding to the  $\text{NO}_3^-$  spikes of interest in this study observed in surface snow on 22–24 November, 13 December, and 25 January. We present results for simulations with and without SPEs for completeness, noting that differences are negligible (never exceeding 0.2%), once again supporting the conclusion that enhanced  $\text{NO}_3^-$  concentrations on these days are not related to SPEs.

### 3.6. Alternative Explanations for Nitrate Spikes

The WACCM simulations provide evidence that nitrate spikes not readily accounted for by soluble ion correlations may nonetheless be related to tropospheric sources. Figure 10 shows the time evolution of vertical profiles of  $\text{NO}_x$  and  $\text{HNO}_3$  above Summit from November through January. Elevated  $\text{NO}_x$ , with a lifetime on the order of



days, indicates relatively fresh pollution sources.  $\text{HNO}_3$ , a product of  $\text{NO}_x$  oxidation with a lifetime on the order of months, is more characteristic of aged plumes. WACCM calculates enhanced  $\text{NO}_x$  and  $\text{HNO}_3$  in the lower troposphere during 22–24 November. High levels of  $\text{NO}_x$  in the middle to upper troposphere occur around 14 December. Elevated levels of both  $\text{NO}_x$  and  $\text{HNO}_3$  are present in the lower to middle troposphere on 25 January.

Figure 11 presents isobaric maps of  $\text{NO}_x$  and  $\text{NO}_y$  from WACCM, identifying polluted continental plumes corresponding to vertical enhancements above Summit. Figure 11a depicts  $\text{NO}_x$  at 800 hPa (~1.5 km) in the lower troposphere above the marine boundary layer 1 day prior to each  $\text{NO}_3^-$  spike not attributable to tropospheric sources. Figure 11b shows  $\text{NO}_y$  plots at 500 hPa (~3.5 km) on days coinciding with these  $\text{NO}_3^-$  spikes. Overlaid vectors indicate the direction and intensity of winds. The WACCM simulations show pollution from Europe reaching Summit on 22 November, with a polluted plume from North America also evident to the south. The middle row in Figure 11 provides a snapshot of a polluted plume traveling from North America at low altitudes on 13 December and aloft over Greenland on 14 December. At altitudes above 5 km (not shown in Figure 11), higher wind speeds steer this plume directly over Summit, consistent with elevated levels of  $\text{NO}_x$  in Figure 10. The simulations show transport of  $\text{NO}_x$  from Europe on 24 January, with a broad region of enhanced  $\text{NO}_y$  over Greenland on 25 January. These model simulations of continental plumes suggest that nitrate spikes in surface snow during these time periods are more likely the result of continental anthropogenic pollution than SPEs.

#### 4. Conclusions

This study screens a 2 year data set of daily measurements of ions in surface snow at Summit, Greenland, from 2000 to 2001 for known tropospheric sources followed by a search for evidence of solar proton events in nitrate records. WACCM modeling simulations examine transport, chemistry, and deposition during three specific time periods when correlations between nitrate and other soluble ions are inconsistent with tropospheric sources. The model calculations confirm that solar proton events significantly impact  $\text{HO}_x$ ,  $\text{NO}_x$ , and  $\text{O}_3$  levels in the mesosphere and stratosphere during the weeks and months after the major 9 November 2000 solar proton event. However, the simulation provides no evidence that SPE-enhanced  $\text{NO}_y$  within the atmospheric column is large enough to account for the observed nitrate peaks in surface snow.

We see no convincing evidence that SPEs are related to impulsive nitrate spikes in surface snow at Summit in the winter of 2000 to 2001 but suggest that spikes not readily accounted for by soluble ion correlations are the result of deposition from polluted plumes originating in North America and Europe. This conclusion is particularly compelling for recent decades when anthropogenic emissions are capable of modifying nitrate levels in the Northern Hemisphere.

The limited SPE enhancement of total column  $\text{NO}_y$  (5% vortex-averaged and 20% local maxima) leads us to conclude that impulsive spikes of  $\text{NO}_3^-$  at the surface are unlikely to result from SPEs similar in magnitude to the 9 November 2000 SPE. It would be worthwhile, however, to consider how large an event would be necessary to produce  $\text{NO}_3^-$  levels at the surface discernible from tropospheric sources as well as the likelihood of such events given the limits of solar flare energy [Aulanier *et al.*, 2013].

A promising alternative to nitrate in the search for proxies for historical SPEs remains the study of cosmogenic radionuclides such as Carbon-14 ( $^{14}\text{C}$ ) and Beryllium-10 ( $^{10}\text{Be}$ ) [Steinhilber *et al.*, 2012]. Measurements of the cosmogenic radionuclide Beryllium-7 ( $^7\text{Be}$ ) are available from Summit from 1997 to 1998, 2000 to 2002, and 2003 to the present [Dibb, 2007]. Although too short lived to serve as a historical proxy, measurements and model comparisons of  $^7\text{Be}$  following recent SPEs would provide insight into vertical transport and deposition processes, paving the way for modeling studies involving longer-lived cosmogenic radionuclides in the context of solar particle events.

Although this study could not definitively link surface observations with solar energetic protons impacting the upper atmosphere, WACCM results once again point to significant impacts of SPEs on the middle and upper atmospheric concentrations of  $\text{HO}_x$ ,  $\text{NO}_x$ , and  $\text{O}_3$ , adding to the growing collection of satellite observations and modeling experiments that strive to clarify perturbations in the chemistry, radiation budget, and dynamics of the atmosphere resulting from solar variability. The quest for an alternate proxy to nitrate for studying solar activity through history remains compelling, particularly with regard to protecting technological infrastructure, understanding climate, and validating predictive models for space weather.

### Acknowledgments

This work was supported by NSF grant 1135432 to the University of New Hampshire. We would like to acknowledge high-performance computing support from Yellowstone (ark:/85065/d7wd3xhc) provided by NCAR's Computational and Information Systems Laboratory, sponsored by the National Science Foundation [Computational and Information Systems Laboratory, 2012; The NCAR Command Language, 2013]. The CESM project is supported by the National Science Foundation and the Office of Science (BER) of the U.S. Department of Energy. The model results and observations used to produce the analysis and figures within this study are available upon request from the corresponding author. We thank the reviewers of the manuscript for their helpful comments and suggestions.

### References

- Aulanier, G., P. Démoulin, C. J. Schrijver, M. Janvier, E. Pariat, and B. Schmieder (2013), The standard flare model in three dimensions II. Upper limit on solar flare energy, *Astron. Astrophys.*, *549*(A66), doi:10.1051/0004-6361/201220406.
- Barnard, L., M. Lockwood, M. A. Hapgood, M. J. Owens, C. J. Davis, and F. Steinhilber (2011), Predicting space climate change, *Geophys. Res. Lett.*, *38*, L16103, doi:10.1029/2011GL048489.
- Bartels-Rausch, T., et al. (2012), Relationship between snow microstructure and physical and chemical processes, *Atmos. Chem. Phys. Discuss.*, *12*, 30,409–30,541, doi:10.5194/acpd-12-30409-2012.
- Bergin, M. H., J.-L. Jaffrezo, C. I. Davidson, J. E. Dibb, S. N. Pandis, R. Hillamo, W. Maenhaut, H. D. Kuhns, and T. Makela (1995), The contributions of snow, fog, and dry deposition to the summer flux of anions and cations at Summit, Greenland, *J. Geophys. Res.*, *100*(D8), 16,275–16,288, doi:10.1029/95JD01267.
- Brakebusch, M., C. E. Randall, D. E. Kinnison, S. Tilmes, M. L. Santee, and G. L. Manney (2013), Evaluation of Whole Atmosphere Community Climate Model simulations of ozone during Arctic winter 2004–2005, *J. Geophys. Res. Atmos.*, *118*, 2673–2688, doi:10.1002/jgrd.50226.
- Burkhardt, J. F., M. Hutterli, R. C. Bales, and J. R. McConnell (2004), Seasonal accumulation timing and preservation of nitrate in firn at Summit, Greenland, *J. Geophys. Res.*, *109*, D19302, doi:10.1029/2004JD004658.
- Calisto, M., P. T. Verronen, E. Rozanov, and T. Peter (2012), Influence of a Carrington-like event on the atmospheric chemistry, temperature and dynamics, *Atmos. Chem. Phys.*, *12*(18), 8679–8686, doi:10.5194/acp-12-8679-2012.
- Committee for the Extension of the U.S. Standard Atmosphere (1976), *U.S. Standard Atmosphere, 1976*, U.S. Government Printing Office, Washington, D. C.
- Computational and Information Systems Laboratory (2012), Yellowstone: IBM iDataPlex system (University Community Computing), Natl. Cent. for Atmos. Res., Boulder, Colo. [Available at <http://n2t.net/ark:/85065/d7wd3xhc>.]
- Crutzen, P. J., I. S. A. Isaksen, and G. C. Reid (1975), Solar proton events—Stratospheric sources of nitric oxide, *Science*, *189*(4201), 457–459, doi:10.1126/science.189.4201.457.
- Damiani, A., M. Storini, C. Rafanelli, and P. Diego (2010), The hydroxyl radical as an indicator of SEP fluxes in the high-latitude terrestrial atmosphere, *Adv. Space Res.*, *46*(9), 1225–1235, doi:10.1016/j.asr.2010.06.022.
- Dibb, J. E. (2007), Vertical mixing above Summit, Greenland: Insights into seasonal and high frequency variability from the radionuclide tracers  $^{10}\text{Be}$  and  $^{210}\text{Pb}$ , *Atmos. Environ.*, *41*(24), 5020–5030, doi:10.1016/j.atmos.env.2006.12.005.
- Dibb, J. E., and M. Fahnstock (2004), Snow accumulation, surface height change, and firn densification at Summit, Greenland: Insights from 2 years of in situ observation, *J. Geophys. Res.*, *109*, D24113, doi:10.1029/2003JD004300.
- Dibb, J. E., and J.-L. Jaffrezo (1997), Air-snow exchange investigations at Summit, Greenland: An overview, *J. Geophys. Res.*, *102*(C12), 26,795–26,807, doi:10.1029/96JC0230.
- Dibb, J. E., and S. I. Whitlow (1996), Recent climate anomalies and their impact on snow chemistry at South Pole, 1987–1994, *Geophys. Res. Lett.*, *23*(10), 1115–1118, doi:10.1029/96GL01039.
- Dibb, J. E., R. W. Talbot, and M. H. Bergin (1994), Soluble acidic species in air and snow at Summit, Greenland, *Geophys. Res. Lett.*, *21*(15), 1627–1630, doi:10.1029/94GL01031.
- Dibb, J. E., R. W. Talbot, S. I. Whitlow, M. C. Shipham, J. Winterle, J. McConnell, and R. Bales (1996), Biomass burning signatures in the atmosphere and snow at Summit, Greenland: An event on 5 August 1994, *Atmos. Environ.*, *30*(4), 553–561, doi:10.1016/1352-2310(95)00328-2.
- Dibb, J. E., R. W. Talbot, J. W. Munger, D. J. Jacob, and S.-M. Fan (1998), Air-snow exchange of  $\text{HNO}_3$  and  $\text{NO}_x$  at Summit, Greenland, *J. Geophys. Res.*, *103*(D3), 3475–3486, doi:10.1029/97JD03132.
- Dibb, J. E., M. Arsenaault, M. C. Peterson, and R. E. Honrath (2002), Fast nitrogen oxide photochemistry in Summit, Greenland snow, *Atmos. Environ.*, *36*(15), 2501–2511, doi:10.1016/S1352-2310(02)00130-9.
- Dibb, J. E., E. Scheuer, M. Avery, J. Plant, and G. Sachse (2006), In situ evidence for renitrification in the Arctic lower stratosphere during the polar aura validation experiment (PAVE), *Geophys. Res. Lett.*, *33*, L12815, doi:10.1029/2006GL026243.
- Dibb, J. E., S. I. Whitlow, and M. Arsenaault (2007), Seasonal variations in the soluble ion content of snow at Summit, Greenland: Constraints from three years of daily surface snow samples, *Atmos. Environ.*, *41*(24), 5007–5019, doi:10.1016/j.atmosenv.2006.12.010.
- Dreschhoff, G. A. M., and E. J. Zeller (1990), Evidence of individual solar proton events in Antarctic snow, *Sol. Phys.*, *127*(2), 333–346, doi:10.1007/BF00152172.
- Dunkerton, T. J., and D. P. Delisi (1986), Evolution of potential vorticity in the winter stratosphere of January–February 1979, *J. Geophys. Res.*, *91*(D1), 1199–1208, doi:10.1029/JD091iD01p01199.
- Emmons, L. K., et al. (2010), Description and evaluation of the Model for Ozone and Related chemical Tracers, version 4 (MOZART-4), *Geosci. Model Dev.*, *3*, 43–67, doi:10.5194/gmd-3-4-2010.
- Fahey, D. W., et al. (2001), The detection of large  $\text{HNO}_3$ -containing particles in the winter Arctic stratosphere, *Science*, *291*(5506), 1026–1031, doi:10.1126/science.1057265.
- Fibiger, D. L., M. G. Hastings, J. E. Dibb, and L. G. Huey (2013), The preservation of atmospheric nitrate in snow at Summit, Greenland, *Geophys. Res. Lett.*, *40*, 3484–3489, doi:10.1002/grl.50659.
- Funke, B., et al. (2011), Composition changes after the “Halloween” solar proton event: The High Energy Particle Precipitation in the Atmosphere (HEPPA) model versus MIPAS data intercomparison study, *Atmos. Chem. Phys.*, *11*(17), 9089–9139, doi:10.5194/acp-11-9089-2011.
- García, R. R., D. R. Marsh, D. E. Kinnison, B. A. Boville, and F. Sassi (2007), Simulation of secular trends in the middle atmosphere, 1950–2003, *J. Geophys. Res.*, *112*, D09301, doi:10.1029/2006JD007485.
- Granier, C., et al. (2005), POET, a database of surface emissions of ozone precursors. [Available at <http://www.aero.jussieu.fr/projet/ACCENT/POET.php>.] GEIA/ACCENT database.
- Grannas, A. M., et al. (2007), An overview of snow photochemistry: Evidence, mechanisms and impacts, *Atmos. Chem. Phys.*, *7*(16), 4329–4373, doi:10.5194/acp-7-4329-2007.
- Gray, L. J., et al. (2010), Solar influences on climate, *Rev. Geophys.*, *48*, RG4001, doi:10.1029/2009RG000282.
- Harvey, V. L., R. B. Pierce, T. D. Fairlie, and M. H. Hitchman (2002), A climatology of stratospheric polar vortices and anticyclones, *J. Geophys. Res.*, *107*(D20), 4442, doi:10.1029/2001JD001471.
- Honrath, R. E., M. C. Peterson, S. Guo, J. E. Dibb, P. B. Shepson, and B. Campbell (1999), Evidence of  $\text{NO}_x$  production within or upon ice particles in the Greenland snowpack, *Geophys. Res. Lett.*, *26*(6), 695–698, doi:10.1029/1999GL900077.
- Horowitz, L. W., et al. (2003), A global simulation of tropospheric ozone and related tracers: Description and evaluation of MOZART, version 2, *J. Geophys. Res.*, *108*(D24), 4784, doi:10.1029/2002JD002853.
- Huff, D. M., P. L. Joyce, G. J. Fochesatto, and W. R. Simpson (2011), Deposition of dinitrogen pentoxide,  $\text{N}_2\text{O}_5$ , to the snowpack at high latitudes, *Atmos. Chem. Phys.*, *11*, 4929–4938, doi:10.5194/acp-11-4929-2011.

- Jackman, C. H., J. E. Frederick, and R. S. Stolarski (1980), Production of odd nitrogen in the stratosphere and mesosphere: An intercomparison of source strengths, *J. Geophys. Res.*, *85*(C12), 7495–7505, doi:10.1029/JC085iC12p07495.
- Jackman, C. H., M. T. Deland, G. J. Labow, E. L. Fleming, D. K. Weisenstein, M. K. W. Ko, M. Sinnhuber, and J. M. Russell (2005), Neutral atmospheric influences of the solar proton events in October–November 2003, *J. Geophys. Res.*, *110*, A09S27, doi:10.1029/2004JA010888.
- Jackman, C. H., et al. (2008), Short- and medium-term atmospheric constituent effects of very large solar proton events, *Atmos. Chem. Phys.*, *8*(3), 765–785, doi:10.5194/acp-8-765-2008.
- Jackman, C. H., D. R. Marsh, F. M. Vitt, R. R. Garcia, C. E. Randall, E. L. Fleming, and S. M. Frith (2009), Long-term middle atmospheric influence of very large solar proton events, *J. Geophys. Res.*, *114*, D11304, doi:10.1029/2008JD011415.
- Jackman, C. H., et al. (2011), Northern Hemisphere atmospheric influence of the solar proton events and ground level enhancement in January 2005, *Atmos. Chem. Phys.*, *11*(13), 6153–6166, doi:10.5194/acp-11-6153-2011.
- Kahl, J. D., D. A. Martinez, H. Kuhns, C. I. Davidson, J.-L. Jaffrezo, and J. M. Harris (1997), Air mass trajectories to Summit, Greenland: A 44-year climatology and some episodic events, *J. Geophys. Res.*, *102*(C12), 26,861–26,875, doi:10.1029/97JC00296.
- Kawa, S. R., J. B. Kumer, A. R. Douglass, A. E. Roche, S. E. Smith, F. W. Taylor, and D. J. Allen (1995), Missing chemistry of reactive nitrogen in the upper stratospheric polar winter, *Geophys. Res. Lett.*, *22*(19), 2629–2632, doi:10.1029/95GL02336.
- Kepko, L., H. Spence, D. F. Smart, and M. A. Shea (2009), Interhemispheric observations of impulsive nitrate enhancements associated with the four large ground-level solar cosmic ray events (1940–1950), *J. Atmos. Sol. Terr. Phys.*, *71*(17–18), 1840–1845, doi:10.1016/j.jastp.2009.07.002.
- Kinnison, D. E., et al. (2007), Sensitivity of chemical tracers to meteorological parameters in the MOZART-3 chemical transport model, *J. Geophys. Res.*, *112*, D20302, doi:10.1029/2006JD007879.
- Kondo, Y., H. Irie, M. Koike, and G. E. Bodeker (2000), Denitrification and nitrification in the Arctic stratosphere during the winter of 1996–1997, *Geophys. Res. Lett.*, *27*(3), 337–340, doi:10.1029/1999GL011081.
- Kvissel, O.-K., Y. J. Orsolini, F. Stordal, I. S. A. Isaksen, and M. L. Santee (2012), Formation of stratospheric nitric acid by a hydrated ion cluster reaction: Implications for the effect of energetic particle precipitation on the middle atmosphere, *J. Geophys. Res.*, *117*, D16301, doi:10.1029/2011JD017257.
- Lamarque, J.-F., et al. (2012), CAM-chem: Description and evaluation of interactive atmospheric chemistry in the Community Earth System Model, *Geosci. Model Dev.*, *5*(2), 369–411, doi:10.5194/gmd-5-369-2012.
- Legrand, M., and M. De Angelis (1996), Light carboxylic acids in Greenland ice: A record of past forest fires and vegetation emissions from the boreal zone, *J. Geophys. Res.*, *101*(D2), 4129–4145, doi:10.1029/95JD03296.
- Legrand, M. R., and R. J. Delmas (1986), Relative contributions of tropospheric and stratospheric sources to nitrate in Antarctic snow, *Tellus B*, *38*(3–4), 236–249, doi:10.1111/j.1600-0889.1986.tb00190.x.
- Legrand, M. R., and S. Kirchner (1990), Origins and variations of nitrate in south polar precipitation, *J. Geophys. Res.*, *95*(D4), 3493–3507, doi:10.1029/JD095iD04p03493.
- Legrand, M. R., F. Stordal, I. S. A. Isaksen, and B. Rognerud (1989), A model study of the stratospheric budget of odd nitrogen, including effects of solar cycle variations, *Tellus B*, *41*(B4), 413–426, doi:10.1111/j.1600-0889.1989.tb00318.x.
- Legrand, M., M. De Angelis, T. Staffelbach, A. Neftel, and B. Stauffer (1992), Large perturbations of ammonium and organic acids content in the summit-Greenland Ice Core: Fingerprint from forest fires?, *Geophys. Res. Lett.*, *19*(5), 473–475, doi:10.1029/91GL03121.
- Legrand, M., A. Léopold, and F. Dominé (1996), Acidic gases (HCl, HF, HNO<sub>3</sub>, HCOOH, and CH<sub>3</sub>COOH): A review of ice core data and some preliminary discussions on their air-snow relationships, in *Chemical Exchange Between the Atmosphere and Polar Snow*, edited by E. W. Wolff and R. C. Bales, pp. 19–43, Springer-Verlag, Berlin, Germany.
- López-Puertas, M., B. Funke, S. Gil-López, T. von Clarmann, G. P. Stiller, M. Höpfner, S. Kellmann, H. Fischer, and C. H. Jackman (2005), Observation of NO<sub>x</sub> enhancement and ozone depletion in the Northern and Southern Hemispheres after the October–November 2003 solar proton events, *J. Geophys. Res.*, *110*, A09S43, doi:10.1029/2005JA011050.
- Manney, G. L., M. L. Santee, L. Froidevaux, K. Hoppel, N. J. Livesey, and J. W. Waters (2006), EOS MLS observations of ozone loss in the 2004–2005 Arctic winter, *Geophys. Res. Lett.*, *33*, L04802, doi:10.1029/2005GL024494.
- Marsh, D. R., R. R. Garcia, D. E. Kinnison, B. A. Boville, F. Sassi, S. C. Solomon, and K. Matthes (2007), Modeling the whole atmosphere response to solar cycle changes in radiative and geomagnetic forcing, *J. Geophys. Res.*, *112*, D23306, doi:10.1029/2006JD008306.
- Marsh, D. R., M. J. Mills, D. E. Kinnison, J.-F. Lamarque, N. Calvo, and L. M. Polvani (2013), Climate change from 1850 to 2005 simulated in CESM1(WACCM), *J. Clim.*, *26*(19), 7372–7391, doi:10.1175/JCLI-D-12-00558.1.
- Mayewski, P. A., W. B. Lyons, M. J. Spencer, M. S. Twickler, C. F. Buck, and S. Whitlow (1990), An ice-core record of atmospheric response to anthropogenic sulphate and nitrate, *Nature*, *346*, 554–556, doi:10.1038/346554a0.
- McCracken, K. G., G. A. M. Dreschhoff, E. J. Zeller, D. F. Smart, and M. A. Shea (2001a), Solar cosmic ray events for the period 1561–1994: 1. Identification in polar ice, 1561–1950, *J. Geophys. Res.*, *106*(A10), 21,585–21,598, doi:10.1029/2000JA000237.
- McCracken, K. G., G. A. M. Dreschhoff, D. F. Smart, and M. A. Shea (2001b), Solar cosmic ray events for the period 1561–1994: 2. The Gleissberg periodicity, *J. Geophys. Res.*, *106*(A10), 21,599–21,609, doi:10.1029/2000JA000238.
- Motizuki, Y., et al. (2009), An Antarctic ice core recording both supernovae and solar cycles, arXiv, 0902.3446. [Available at <http://arXiv.org/abs/0902.3446>.]
- National Research Council (2008), *Severe Space Weather Events—Understanding Societal and Economic Impacts: A Workshop Report*, The National Academies Press, Washington, D. C.
- National Research Council (2012), *The Effects of Solar Variability on Earth's Climate: A Workshop Report*, The National Academies Press, Washington, D. C.
- Neale, R. B., J. Richter, S. Park, P. H. Lauritzen, S. J. Vavrus, P. J. Rasch, and M. Zhang (2013), The mean climate of the Community Atmosphere Model (CAM4) in forced SST and fully coupled experiments, *J. Clim.*, *26*, 5150–5168, doi:10.1175/JCLI-D-12-00236.1.
- Neu, J. L., and M. J. Prather (2012), Toward a more physical representation of precipitation scavenging in global chemistry models: Cloud overlap and ice physics and their impact on tropospheric ozone, *Atmos. Chem. Phys.*, *12*(7), 3289–3310, doi:10.5194/acp-12-3289-2012.
- Ogurtsov, M. G., and M. Oinonen (2014), Evidence of the solar Gleissberg cycle in the nitrate concentration in polar ice, *J. Atmos. Sol. Terr. Phys.*, *109*, 37–42, doi:10.1016/j.jastp.2013.12.017.
- Päivärinta, S.-M., A. Seppälä, M. E. Andersson, P. T. Verronen, L. Thölix, and E. Kyrölä (2013), Observed effects of solar proton events and sudden stratospheric warmings on odd nitrogen and ozone in the polar middle atmosphere, *J. Geophys. Res. Atmos.*, *118*, 6837–6848, doi:10.1002/jgrd.50486.
- Palmer, A. S., T. D. Van Ommen, M. A. J. Curran, and V. Morgan (2001), Ice-core evidence for a small solar-source of atmospheric nitrate, *Geophys. Res. Lett.*, *28*(10), 1953–1956, doi:10.1029/2000GL012207.
- Popp, P. J., et al. (2001), Severe and extensive denitrification in the 1999–2000 Arctic winter stratosphere, *Geophys. Res. Lett.*, *28*(15), 2875–2878, doi:10.1029/2001GL013132.
- Porter, H. S., C. H. Jackman, and A. E. S. Green (1976), Efficiencies for production of atomic nitrogen and oxygen by relativistic proton impact in air, *J. Chem. Phys.*, *65*, 154–167, doi:10.1063/1.432812.

- Randall, C. E., et al. (2002), Validation of POAM III NO<sub>2</sub> measurements, *J. Geophys. Res.*, 107(D20), 4432, doi:10.1029/2001JD001520.
- Randall, C. E., et al. (2005), Stratospheric effects of energetic particle precipitation in 2003–2004, *Geophys. Res. Lett.*, 32, L05802, doi:10.1029/2004GL022003.
- Randall, C. E., V. L. Harvey, C. S. Singelton, S. M. Bailey, P. F. Bernath, M. Codrescu, H. Nakajima, and J. M. Russell III (2007), Energetic particle precipitation effects on the Southern Hemisphere stratosphere in 1992–2005, *J. Geophys. Res.*, 112, D08308, doi:10.1029/2006JD007696.
- Randall, C. E., V. L. Harvey, D. E. Siskind, J. France, P. F. Bernath, C. D. Boone, and K. A. Walker (2009), NO<sub>x</sub> descent in the Arctic middle atmosphere in early 2009, *Geophys. Res. Lett.*, 36, L18811, doi:10.1029/2009GL039706.
- Rasch, P. J., N. M. Mahowald, and B. E. Eaton (1997), Representations of transport, convection, and the hydrologic cycle in chemical transport models: Implications for the modeling of short-lived and soluble species, *J. Geophys. Res.*, 102(D23), 28,127–28,138, doi:10.1029/97JD02087.
- Rienecker, M. M., et al. (2011), MERRA: NASA's Modern-Era Retrospective Analysis for Research and Applications, *J. Clim.*, 24(14), 3624–3648, doi:10.1175/JCLI-D-11-00015.1.
- Riley, P. (2012), On the probability of occurrence of extreme space weather events, *Space Weather*, 10, S02012, doi:10.1029/2011SW000734.
- Röthlisberger, R., M. Bigler, M. Hutterli, S. Sommer, B. Stauffer, H. G. Junghans, and D. Wagenbach (2000), Technique for continuous high-resolution analysis of trace substances in firn and ice cores, *Environ. Sci. Technol.*, 34(2), 338–342, doi:10.1021/es9907055.
- Röthlisberger, R., et al. (2002), Nitrate in Greenland and Antarctic ice cores: A detailed description of post-depositional processes, *Ann. Glaciol.*, 35, 209–216, doi:10.3189/172756402781817220.
- Rusch, D. W., J. C. Gérard, S. Solomon, P. J. Crutzen, and G. C. Reid (1981), The effect of particle precipitation events on the neutral and ion chemistry of the middle atmosphere. I—Odd nitrogen, *Planet. Space Sci.*, 29(7), 767–774, doi:10.1016/0032-0633(81)90048-9.
- Santee, M. L., G. L. Manney, N. J. Livesey, and J. W. Waters (2000), UARS Microwave Limb Sounder observations of denitrification and ozone loss in the 2000 Arctic late winter, *Geophys. Res. Lett.*, 27(19), 3213–3216, doi:10.1029/2000GL011738.
- Savarino, J., and M. Legrand (1998), High northern latitude forest fires and vegetation emissions over the last millennium inferred from the chemistry of a central Greenland ice core, *J. Geophys. Res.*, 103(D7), 8267–8279, doi:10.1029/97JD03748.
- Schrijver, C. J., et al. (2012), Estimating the frequency of extremely energetic solar events, based on solar, stellar, lunar, and terrestrial records, *J. Geophys. Res.*, 117, A08103, doi:10.1029/2012JA017706.
- Semeniuk, K., J. C. McConnell, and C. H. Jackman (2005), Simulation of the October–November 2003 solar proton events in the CMAM GCM: Comparison with observations, *Geophys. Res. Lett.*, 32, L15502, doi:10.1029/2005GL022392.
- Shea, M. A., D. F. Smart, K. G. McCracken, G. A. M. Dreschhoff, and H. E. Spence (2006), Solar proton events for 450 years: The Carrington event in perspective, *Adv. Space Res.*, 38(2), 232–238, doi:10.1016/j.asr.2005.02.100.
- Sigg, A., K. Fuhrer, M. Anklin, T. Staffelbach, and D. Zurmuehle (1994), A continuous analysis technique for trace species in ice cores, *Environ. Sci. Technol.*, 28(2), 204–209, doi:10.1021/es00051a004.
- Silvente, E. (1993), Contribution à l'étude de la fonction de transfert air neige en régions polaires, PhD thesis, Université Joseph Fourier, Grenoble, France.
- Silvente, E., and M. Legrand (1995), A preliminary study of the air–snow relationship for nitric acid in Greenland, in *Ice Core Studies of Global Biogeochemical Cycles*, edited by R. J. Delmas, pp. 225–240, Springer, Berlin-Heidelberg, Germany.
- Smart, D. F., and M. A. Shea (1994), Geomagnetic cutoffs: A review for space dosimetry applications, *Adv. Space Res.*, 14(10), 787–796, doi:10.1016/0273-1177(94)90543-6.
- Solomon, S., D. W. Rusch, J. C. Gerard, G. C. Reid, and P. J. Crutzen (1981), The effect of particle precipitation events on the neutral and ion chemistry of the middle atmosphere. II—Odd hydrogen, *Planet. Space Sci.*, 29(8), 885–893, doi:10.1016/0032-0633(81)90078-7.
- Steinhilber, F., et al. (2012), 9,400 years of cosmic radiation and solar activity from ice cores and tree rings, *Proc. Natl. Acad. Sci. U.S.A.*, 109(16), 5967–5971, doi:10.1073/pnas.1118965109.
- Sturm, M., and C. S. Benson (1997), Vapor transport, grain growth and depth-hoar development in the subarctic snow, *J. Glaciol.*, 43(143), 42–59.
- Taylor, K. E., R. J. Stouffer, and G. A. Meehl (2012), An overview of CMIP5 and the experiment design, *Bull. Am. Meteorol. Soc.*, 93(4), 485–498, doi:10.1175/BAMS-D-11-00094.1.
- The NCAR Command Language (Version 6.1.1) [Software] (2013), Boulder, Colorado: UCAR/NCAR/CISL/VETS, doi:10.5065/D6WD3XH5.
- Traversi, R., I. G. Usoskin, S. K. Solanki, S. Becagli, M. Frezzotti, M. Severi, B. Stenni, and R. Udisti (2012), Nitrate in polar ice: A new tracer of solar variability, *Sol. Phys.*, 280, 237–254, doi:10.1007/s11207-012-0060-3.
- van der Werf, G. R., J. T. Randerson, L. Giglio, G. J. Collatz, P. S. Kasibhatla, and A. F. Arellano Jr. (2006), Interannual variability in global biomass burning emissions from 1997 to 2004, *Atmos. Chem. Phys.*, 6, 3423–3441, doi:10.5194/acp-6-3423-2006.
- Verronen, P. T., B. Funke, M. López-Puertas, G. P. Stiller, T. von Clarmann, N. Glatthor, C.-F. Enell, E. Turunen, and J. Tamminen (2008), About the increase of HNO<sub>3</sub> in the stratopause region during the Halloween 2003 solar proton event, *Geophys. Res. Lett.*, 35, L20809, doi:10.1029/2008GL035312.
- Vitt, F. M., and C. H. Jackman (1996), A comparison of sources of odd nitrogen production from 1974 through 1993 in the Earth's middle atmosphere as calculated using a two-dimensional model, *J. Geophys. Res.*, 101(D3), 6729–6739, doi:10.1029/95JD03386.
- Waibel, A. E., T. Peter, K. S. Carslaw, H. Oelhaf, G. Wetzal, P. J. Crutzen, U. Poschl, A. Tsias, E. Reimer, and H. Fischer (1999), Arctic ozone loss due to denitrification, *Science*, 283(5410), 2064–2069, doi:10.1126/science.283.5410.2064.
- Wegner, T., D. E. Kinnison, R. R. Garcia, and S. Solomon (2013), Simulation of polar stratospheric clouds in the specified dynamics version of the Whole Atmosphere Community Climate Model, *J. Geophys. Res. Atmos.*, 118, 4991–5002, doi:10.1002/jgrd.50415.
- Weller, R., D. Wagenbach, M. Legrand, C. Elsässer, X. Tian-Kunze, and G. König-Langlo (2011), Continuous 25-yr aerosol records at coastal Antarctica—I: Inter-annual variability of ionic compounds and links to climate indices, *Tellus B*, 63, 901–919, doi:10.1111/j.1600-0889.2011.00542.x.
- Whitlow, S., P. Mayewski, J. Dibb, G. Holdsworth, and M. Twickler (1994), An ice-core-based record of biomass burning in the Arctic and Subarctic, 1750–1980, *Tellus B*, 46(3), 234–242, doi:10.1034/j.1600-0889.1994.t01-2-00006.x.
- Wolff, E. W. (1995), Nitrate in polar ice, in *Ice Core Studies of Global Biogeochemical Cycles*, edited by R. J. Delmas, pp. 195–224, Springer, Berlin, Germany.
- Wolff, E. W., A. E. Jones, S. J.-B. Bauguitte, and R. A. Salmon (2008), The interpretation of spikes and trends in concentration of nitrate in polar ice cores, based on evidence from snow and atmospheric measurements, *Atmos. Chem. Phys.*, 8(18), 5627–5634, doi:10.5194/acp-8-5627-2008.
- Wolff, E. W., M. Bigler, M. A. J. Curran, J. E. Dibb, M. M. Frey, M. Legrand, and J. R. McConnell (2012), The Carrington event not observed in most ice core nitrate records, *Geophys. Res. Lett.*, 39, L08503, doi:10.1029/2012GL051603.
- Zeller, E. J., and G. A. M. Dreschhoff (1995), Anomalous nitrate concentrations in polar ice cores—Do they result from solar particle injections into the polar atmosphere?, *Geophys. Res. Lett.*, 22(18), 2521–2524, doi:10.1029/95GL02560.
- Zeller, E. J., and B. C. Parker (1981), Nitrate ion in Antarctic firn as a marker for solar activity, *Geophys. Res. Lett.*, 8(8), 895–898, doi:10.1029/GL008i008p00895.